
Generative Modeling by Value-Driven Transport

Pablo Moreno-Muñoz *
Universitat Pompeu Fabra
Barcelona, Spain
pablo.moreno@upf.edu

Adrian Müller *
ETH Zürich
Zürich, Switzerland
adrian.mueller@inf.ethz.ch

Gergely Neu *
ICREA & Universitat Pompeu Fabra
Barcelona, Spain
gergely.neu@gmail.com

Abstract

We propose a new framework for generative modeling based on a discrete-time stochastic control formulation of measure transport. Adapting classic results from control theory, we formulate our problem as a linear program whose dual variables correspond to the *optimal value function* of the control problem, which directly encodes the optimal control policy. Exploiting this LP formulation, we develop an efficient simulation-free primal-dual algorithm for computing approximately optimal value functions and the associated *value-driven transport* (VDT) policies which approximate the true optimal policy. We show that well-trained VDT policies enjoy numerous favorable properties in comparison with other state-of-the-art methods based on flows, diffusions, or Schrödinger bridges: they lead to straight transport paths which can be simulated quickly and robustly, and can be enhanced in all the same ways as diffusion and flow-based models (e.g., conditional generation, classifier-free guidance, unpaired data-to-data translation are all easy to incorporate). We evaluate our methodology in a range of experiments, with results that indicate strong performance and good potential for scalability.

1 Introduction

Many modern generative modeling tasks can be naturally formulated as problems of measure transport, whereby one seeks a transformation that turns samples from a given source distribution into samples from a desired target distribution. The rich literature on optimal transport (OT, [59, 46, 42]) provides solid mathematical foundations for formulating such measure transport problems and characterizing their solutions, making it a natural starting point for developing computational methods for generative modeling. In this work, we introduce a new algorithmic framework that approximates optimal transport plans by combining tools from modern deep learning and optimal control.

The core of our methodology is a reformulation of the classic *dynamic optimal transport* problem of Benamou and Brenier [6] as a discrete-time stochastic control problem, where an initial state distribution is steered by a control policy in a fixed number of H decision rounds, aiming to hit the target distribution at the final round while minimizing movement cost along the way. Using classic tools from control theory, we show that optimal control policies can be written in terms of a *value function*, with the evolution of the states determined by the gradient of the value functions. Motivated by this observation, we consider the class of *value-driven transport* policies that push states along the gradient fields of approximate value functions, and develop an algorithmic framework for computing the values. For this purpose, we adapt a classic linear-programming (LP) formulation of optimal control to our needs, where the optimal dual variables correspond to the optimal value functions.

Our algorithmic contribution is the development of a new primal-dual method for approximately solving this LP—or, equivalently, to find a saddle-point of its Lagrangian. At a high level, our method is based on approximating the associated dual function by numerically optimizing the primal variables and evaluating stochastic gradients with respect to the dual variables using small to moderate minibatches of data. Both primal and dual updates can be performed efficiently, without needing

* Authors listed alphabetically.

access to simulated trajectories from the learned model. The key to this efficiency is parametrizing the primal variables as particle clouds initialized as samples of a stochastic interpolant between the source and target distributions, which are then updated using Wasserstein gradient descent. With this choice, implementing our method only requires a single neural network, used for parametrizing the value functions. We verify the effectiveness of this method in an exhaustive range of experiments, with the results indicating good robustness and scalability properties of the training procedure and convincing performance of the learned transport policies.

Our approach has a number of conceptual and practical advantages over competing methods for generative modeling. The most notable of these are consequences of a well-known valuable property of the optimal solution to the dynamic OT problem: the solution paths generated by the optimal policy are *linear interpolations* of the (appropriately coupled) source and target points. This implies that the optimal policy could in principle be used for generating samples from the target using *just a single step* (since under an optimal policy, all consecutive steps would be done in the same direction, with the same stepsize). While in practice, the level of precision needed for such one-step generation is hard to achieve due to errors of approximation and optimization, our empirical results show that the straight-path property of the optimal policy can indeed be used to radically reduce the number of generation steps at test time, up to a factor of 10 in comparison to the horizon H used at training time. Another appealing property of our method is that it learns the value function as opposed to attempting to directly learn the optimal policy, whose value-driven structure would be challenging to enforce otherwise when working with parametrized approximations. Additionally, since our problem formulation is symmetric with respect to the roles source and target distributions, the learned value functions can be used equally effectively for transport from source to target and vice versa.

The techniques used for deriving and implementing our method are all quite different from the standard tools of the generative modeling literature. Instead of using concepts from continuous-time mathematics (SDEs and their time reversals) and denoising (score functions and their estimation) like nearly all state-of-the-art methods for generative modeling, our approach is rooted in discrete-time stochastic optimal control—a setting more commonly considered under the umbrella of reinforcement learning (RL, [55]). Indeed, our problem formulation can be seen to be equivalent to finding optimal policies in a constrained Markov decision process (MDP, [43, 7]), with the objective of generating from the target being formulated in terms of a constraint. Due to this constraint, our problem cannot be directly addressed with standard tools of RL which are designed for optimizing a single numerical reward function without constraints. Additionally, common RL methods are developed with unknown state dynamics in mind, which makes them unlikely to perform well in our setting where the state dynamics is perfectly known and controllable without restrictions. That said, our algorithm design draws quite a bit of inspiration from the RL literature, particularly from works that use LP formulations as their starting point [49, 13, 4, 33, 37]. In these works, the LP framework has largely been used as a tool for theoretical analysis, and the methods themselves have arguably achieved only limited empirical success so far. Thus, our encouraging experimental results might be seen as a validation that the LP framework can indeed serve as the basis of competitive large-scale learning algorithms. We believe that the techniques we develop here might prove useful in addressing other control tasks in areas such as RL as well.

The rest of the paper is organized as follows. After providing a quick primer on optimal transport in Section 2, we present our framework and algorithm in Section 3, and then Section 4 describes our experiments. The main text is concluded in Section 5.

Notation. We denote the set of (Radon) probability measures on $\mathbb{R}^{d \times d}$ by \mathcal{S} . For a probability distribution $p \in \mathcal{S}$ and a function $f : \mathbb{R}^{d \times d} \rightarrow \mathbb{R}^d$, we use $f_{\#}p$ to denote the pushforward of p under f (i.e., the distribution of $f(X)$ with $X \sim p$), and we extend this definition to arbitrary domains and co-domains of f . We define the maps $\mathcal{F}, \mathcal{B} : \mathbb{R}^d \times \mathbb{R}^d \rightarrow \mathbb{R}^d$ as the projections $\mathcal{B}(x, y) = x$ and $\mathcal{F}(x, y) = y$, which respectively induce the marginalization operators $\mathcal{B}_{\#}$ and $\mathcal{F}_{\#}$ acting on joint distributions. Throughout the paper, equalities between functions are to be understood to hold almost everywhere (a.e.), and minimization over functions as minimization over continuous functions.

2 Preliminaries

We consider the problem of optimal transport (OT) over \mathbb{R}^d with the squared Euclidean distance $\frac{1}{2} \|x - y\|^2$ as transport cost. This is a very well-studied problem with countless equivalent formulations and connections with many areas of mathematics, probability, and physics [59, 46]. Here, we

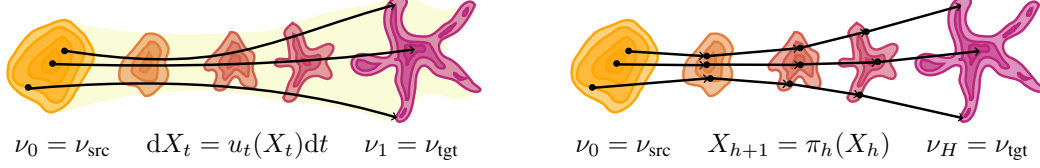


Figure 1: Continuous- and discrete-time transport plans. Continuous-time plans are defined as smooth solutions of ODEs parametrized by a continuous-time control drift, whereas discrete-time plans are defined by a sequence of control policies directly mapping states to next states.

state a few equivalent definitions and basic results that are directly relevant to our own formulation of the problem, which we state in the second half of this section. We refer to the books of Villani [59] and Santambrogio [46] for an exhaustive treatment of the subject, and recommend the notes of Peyré [42], Peyré [41] as a more accessible quick introduction.

Let us consider two measures ν_{src} and ν_{tgt} on \mathbb{R}^d , to be referred to as the *source* and *target* distributions, respectively. We will often refer to $\mathcal{X} = \mathbb{R}^d$ as the *state space* and elements $x \in \mathcal{X}$ as *states*. We assume that both distributions admit densities with respect to the Lebesgue measure, and aim to solve the so-called *Monge problem*²:

$$\mathcal{W}_2^2(\nu_{\text{src}}, \nu_{\text{tgt}}) = \min_{\substack{M: \mathbb{R}^d \rightarrow \mathbb{R}^d \\ M_{\#} \nu_{\text{src}} = \nu_{\text{tgt}}}} \frac{1}{2} \int \|M(x) - x\|^2 d\nu_{\text{src}}(x). \quad (1)$$

This problem is known to admit a unique solution under our conditions specified above, and the value of the minimum is called the *squared Wasserstein-2 distance* between ν_{tgt} and ν_{src} . The distance can equivalently be shown to be the value of the *Kantorovich problem*

$$\mathcal{W}_2^2(\nu_{\text{src}}, \nu_{\text{tgt}}) = \min_{\gamma \in \Gamma(\nu_{\text{src}}, \nu_{\text{tgt}})} \frac{1}{2} \int \|x - y\|^2 d\gamma(x, y), \quad (2)$$

where the domain of optimization is the set of all couplings of ν_{src} and ν_{tgt} : $\Gamma(\nu_{\text{src}}, \nu_{\text{tgt}}) = \{\gamma \in \mathcal{S} \mid \mathcal{B}_{\#} \gamma = \nu_{\text{src}} \wedge \mathcal{F}_{\#} \gamma = \nu_{\text{tgt}}\}$. The minimizer is unique and satisfies $\gamma^* = (\text{id}, M^*)_{\#} \nu_{\text{src}}$.

Another equivalent formulation due to Benamou and Brenier [6] poses the OT problem as a problem of stochastic control. This framework sets up a control problem in which an initial state $X_0 \in \mathbb{R}^d$ is drawn from the source distribution ν_{src} at the initial time instant $t = 0$, and the continuous process of states is then steered by a time-dependent *control drift* $u_t: \mathbb{R}^d \rightarrow \mathbb{R}^d$ according to the continuous-time dynamics $dX_t = u_t(X_t)dt$. We call the control *feasible* if the distribution of the resulting final state X_1 matches the target at time $t = 1$ (i.e., $\text{Law}(X_1) = \nu_{\text{tgt}}$), and denote all such controls by $\mathcal{U}(\nu_{\text{src}}, \nu_{\text{tgt}})$. Denoting the expectation operator under the path distribution induced by u as $\mathbb{E}_u[\cdot]$, the optimal transport cost can be equivalently written as

$$\mathcal{W}_2^2(\nu_{\text{src}}, \nu_{\text{tgt}}) = \min_{u \in \mathcal{U}(\nu_{\text{src}}, \nu_{\text{tgt}})} \frac{1}{2} \int_{[0,1]} \mathbb{E}_u \left[\|u_t(X_t)\|^2 \right] dt. \quad (3)$$

The optimal control can be shown to satisfy $u_t^*(x) = \nabla_x \psi_t^*(x)$ for some scalar *potential function* $\psi^*: [0, 1] \times \mathbb{R}^d \rightarrow \mathbb{R}$. Thus, solving the continuous-time optimal control problem reduces to finding the potential ψ^* . Another fact which will be important for us is that the optimal control paths are linear interpolations of the optimally coupled points $(X_0, X_1) \sim \gamma^*$, with $X_t = (1-t)X_0 + tX_1$ satisfied for all $t \in [0, 1]$.

Our approach is based on a discrete-time analogue of this latter formulation of the OT problem, where a sequence of states are generated recursively over a sequence of discrete *time steps* $h = 0, 1, \dots, H$ (where H is called the *horizon*). The initial state X_0 is drawn from the source distribution ν_{src} , and each consecutive state X_0, X_1, \dots, X_H is selected according to a *control policy* π that maps each state X_h to the next state as $X_{h+1} = \pi_h(X_h)$. The control cost associated with each state transition is $c(X_h, X_{h+1}) = \frac{H+1}{2} \|X_h - X_{h+1}\|^2$. In general, we will consider non-stationary policies represented as the collection of deterministic maps $\pi = \{\pi_h: \mathbb{R}^d \rightarrow \mathbb{R}^d\}_{h=0}^H$. A policy is

²The factor $\frac{1}{2}$ featured in all our definitions is not common in the literature, but will be helpful for our derivations.

called *feasible* if the law of the final state X_{H+1} generated by the above process matches the target distribution ($\text{Law}(X_{H+1}) = \nu_{\text{tgt}}$), and we denote the set of feasible control policies by $\Pi(\nu_{\text{src}}, \nu_{\text{tgt}})$. Letting $\mathbb{E}_\pi[\cdot]$ stand for the expectation operator under the joint distribution of state sequences generated by π , we then set up our objective as

$$\mathcal{W}_2^2(\nu_{\text{src}}, \nu_{\text{tgt}}) = \min_{\pi \in \Pi(\nu_{\text{src}}, \nu_{\text{tgt}})} \frac{H+1}{2} \sum_{h=0}^H \mathbb{E}_\pi \left[\|X_{h+1} - X_h\|^2 \right]. \quad (4)$$

In the following section, we will show that this optimization problem is well-posed, has a unique optimal solution, and its value is equivalent to all the above definitions of the squared Wasserstein-2 distance (as our notation already suggests).

3 Value-driven transport

There are many possible ways to address the discrete-time dynamic OT problem of Equation (4). Unfortunately, since our problem features a hard constraint on the terminal-state distribution, the standard theory of dynamic programming does not apply [5, 22, 7]. Instead, our approach is based on the *linear programming* formulation of discrete-time optimal control, originally developed in a series of papers in the 1960s [34, 14, 16, 15]: we restate our problem as optimization over the space of state distributions that can be generated by feasible control policies, which space is exactly characterized by a set of linear constraints. In Section 3.1 below, we formalize this optimization problem and state several fundamental claims about its solution. Due to space constraints, we only provide the essentials here, and defer the complete statements along with their derivations to Appendix B. Given these foundations, Section 3.2 then describes our main algorithmic contribution: a scalable stochastic optimization method for computing near-optimal solutions of the LP.

3.1 Discrete-time dynamic OT as a linear program

A key concept of our framework is that of *occupancy measures*. The occupancy measure associated with a control policy π is the collection of joint distributions $\mu^\pi = \{\mu_h^\pi \in \Delta_{\mathbb{R}^d \times \mathbb{R}^d}\}_{h=0}^H$ over the state space, with $\mu_h^\pi = \mathbb{P}_\pi[(X_h, X_{h+1}) \in \cdot]$ corresponding to the distribution of the state pair X_h, X_{h+1} generated by policy π under the discrete-time control process described in Section 2. As is well-known in the context of Markov decision processes, the set of all valid occupancy measures that can be induced by control policies is uniquely characterized by a set of linear constraints (see, e.g., Chapter 6.9 in Puterman [43]). Adapting these results to our needs, we formulate our optimal control problem as the following linear program:

$$\begin{aligned} \mathcal{W}_{\text{dyn},2}^2(\nu_{\text{src}}, \nu_{\text{tgt}}) &= \min_{\mu \in \mathcal{S}^{H+1}} \frac{H+1}{2} \sum_{h=0}^H \int \|x - y\|^2 d\mu_h(x, y) \\ \text{s.t.} \quad \nu_{\text{src}} &= \mathcal{B}_\# \mu_0 \\ \mathcal{F}_\# \mu_h &= \mathcal{B}_\# \mu_{h+1} \quad (\forall h \in \{0, \dots, H-1\}) \\ \mathcal{F}_\# \mu_H &= \nu_{\text{tgt}} \end{aligned} \quad (\text{LP})$$

The first and last constraints are called *source* and *target* constraints, and the intermediate ones are called *flow constraints*. Intuitively, these express the criterion that the measures μ_h should be temporally consistent across different time indices h . The single-stage version of the problem ($H = 0$) is clearly equivalent to the Kantorovich problem (2). Our first technical result shows that this remains true for arbitrary choices of H .

Theorem 3.1. *The solution μ^* of (LP) satisfies $\mathcal{W}_{\text{dyn},2}^2(\nu_{\text{src}}, \nu_{\text{tgt}}) = \mathcal{W}_2^2(\nu_{\text{src}}, \nu_{\text{tgt}})$. Moreover:*

- Let γ^* be optimal for the Kantorovich problem (2), define $(X_0, X_{H+1}) \sim \gamma^*$ and let $X_h = X_0 + \frac{h}{H+1}(X_{H+1} - X_0)$. Then the laws μ_h^* of (X_h, X_{h+1}) form an optimal solution μ^* for (LP).
- Suppose that the static Monge problem (1) admits a solution M^* . Then the discrete-time dynamic OT problem (4) admits an optimal solution π^* . Furthermore, μ^* given by $\mu_h^* = (\pi_{h-1}^* \circ \dots \circ \pi_0^*, \pi_h^* \circ \dots \circ \pi_0^*)_\# \nu_{\text{src}}$ and $\mu_0^* = (\text{id}, \pi_0^*)_\# \nu_{\text{src}}$ is an optimal solution for (LP).

Notice that the two claims together imply that the optimal control policy π^* consists of moving each source point along a straight line towards a designated target point, and μ^* represents the probability distributions of the corresponding linearly interpolated states.

Duality. The Lagrangian function associated with (LP) is defined by introducing a set of dual variables $V : \mathbb{R}^d \rightarrow \mathbb{R}$ to enforce the constraints, and adding them to the objective:

$$\mathcal{L}(\mu, V) = \sum_{h=0}^H \int (c(x, y) + V_{h+1}(y) - V_h(x)) d\mu_h(x, y) + \int V_0(x) d\nu_{\text{src}}(x) - \int V_{H+1}(x) d\nu_{\text{tgt}}(x).$$

Then, our problem can be equivalently rewritten as the min-max optimization problem $\mathcal{W}_{\text{dyn},2}^2(\nu_{\text{src}}, \nu_{\text{tgt}}) = \inf_{\mu \in \mathcal{S}^{H+1}} \sup_{V \in \mathcal{C}(\Omega)^{H+2}} \mathcal{L}(\mu, V)$, which can be shown to admit a unique solution (μ^*, V^*) on the transported support.³ Additionally, the optimal dual variables V^* maximize the associated *dual function* defined as $\mathcal{G}(V) = \inf_{\mu \in \mathcal{S}^{H+1}} \mathcal{L}(\mu, V)$. We show below that V^* satisfies a system of equations analogous to the *Bellman optimality equations* from the theory of (unconstrained) optimal control and dynamic programming. By this analogy, we borrow the terminology of dynamic programming and refer to the set of dual variables V as the *value function* and V^* as the *optimal value function*. Crucially, we also show that the optimal value function directly encodes the optimal control policy π^* . These results are stated formally below.

Theorem 3.2. *Let μ^* be an optimal solution for (LP) let V^* be a maximizer of the dual function \mathcal{G} . Then, for all $h = 0, 1, \dots, H$ and for $(\pi_{h-1}^* \circ \dots \circ \pi_0^*)_{\#} \nu_{\text{src}}$ -almost all $x \in \Omega$, the optimal value function and the optimal policy respectively satisfy*

$$\begin{aligned} V_h^*(x) &= \min_{y \in \Omega} \left(\frac{H+1}{2} \|x - y\|^2 + V_{h+1}^*(y) \right), \\ \pi_h^*(x) &= \arg \min_{y \in \Omega} \left(\frac{H+1}{2} \|x - y\|^2 + V_{h+1}^*(y) \right). \end{aligned}$$

Note that, unlike in standard dynamic programming, V_{H+1}^* is typically *not* zero, but rather corresponds to the optimal dual variables that penalize violations of the target-distribution constraint. In this sense, V_{H+1}^* may be seen as a “discriminator” function, which can be shown to correspond to the optimal dual variables of the Kantorovich problem (2). Even more importantly, the theorem shows that the optimal policy is *greedy* with respect to V^* . Generally, a policy π is greedy with respect to a value function V if it maps state x_h to x_{h+1} that satisfies

$$x_{h+1} = \arg \min_{y \in \Omega} \left(\frac{H+1}{2} \|x_h - y\|^2 + V_{h+1}(y) \right) = x_h - \frac{1}{H+1} \nabla_x V_{h+1}(x_{h+1}).$$

Note that this system of equations is not easy to solve, as it features x_{h+1} on both the left- and right-hand side. We address this issue below by making one more important observation about the structure of the optimal solution paths.

Value-driven transport policies. As established in Theorem 3.1, the optimal solution paths linearly interpolate between the target and source points. By combining this insight with the above fact about π^* , we deduce that states sampled from the optimal policy evolve as

$$X_{h+1} = X_h + \frac{1}{H+1} (X_{H+1} - X_0) = X_h - \frac{1}{H+1} \nabla_x V_{h+1}^*(X_{h+1}), \quad (5)$$

which implies that $\nabla_x V_h^*(X_h) = (X_0 - X_{H+1})$ holds for all h . Therefore, the optimal policy can be written explicitly as $\pi_h^*(x) = x - \frac{1}{H+1} \nabla_x V_h^*(x)$, recovering the form of the continuous-time dynamic OT path. Based on this observation, we define the *value-driven transport (VDT) policy* induced by a generic value function V as the policy $\pi(\cdot; V)$ mapping states to next states as

$$\pi_h(x; V) = x - \frac{1}{H+1} \nabla_x V_h(x). \quad (6)$$

Clearly, we have $\pi(\cdot; V^*) = \pi^*$, but note that value-driven and greedy policies do not generally coincide for value functions other than V^* . In contrast to greedy policies, VDT policies have the distinct advantage of being explicitly computable from V^* , while remaining a sufficiently expressive class to include the optimal policy. Therefore, we will restrict our attention to VDT policies in our algorithm design, which we turn to describing below.

³The solution V^* is only unique up to a constant additive shift. For technical reasons, here we restrict the problem to the domains $\mathcal{M} := \mathcal{M}_{\geq 0}(\Omega \times \Omega)$ and $\mathcal{C}(\Omega)$ over a compact convex set $\Omega \subset \mathbb{R}^d$ rather than all of \mathbb{R}^d , by assuming that $\text{supp}(\nu_{\text{src}}), \text{supp}(\nu_{\text{tgt}}) \subset \Omega$. All previous statements then hold analogously.

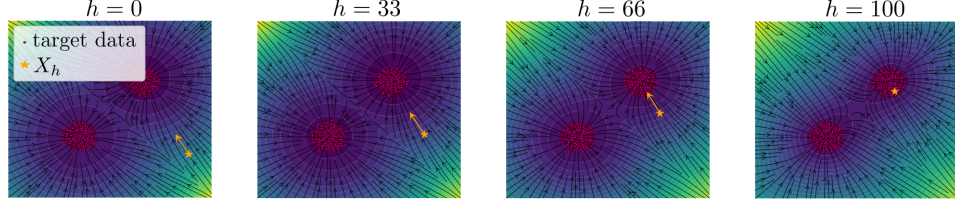


Figure 2: Value functions and value-driven transport policies in a two-dimensional example, plotted for time indices $h \in \{0, 33, 66, 100\}$. A (straight) sample path followed by a source sample and the update directions highlighted in yellow.

3.2 Primal-dual methods for VDT training

We are now ready to describe our main algorithmic contribution: a primal-dual algorithm for computing near-optimal VDT policies. In short, we aim at approximately solving the min-max problem $\inf_{\mu} \sup_V \mathcal{L}(\mu, V)$, and returning the VDT policy induced by the estimated value function. The key practical challenge is picking an appropriate parametrization for the primal and dual variables that allows efficient training while having only sample access to the distributions ν_{src} and ν_{tgt} .

Dual parametrization and update rule. We parametrize the dual variables using a neural network V_{θ} that takes as input a state x and a time index h , and returns $V_{\theta}(x, h) \in \mathbb{R}$. Our ideal goal is to perform stochastic gradient ascent on the dual function \mathcal{G} with respect to the parameters θ . In order to construct a sample-based estimator of the required gradients, we consider a minibatch of (possibly coupled) samples $(X_{\text{src}}(1), \dots, X_{\text{src}}(b)) \sim \nu_{\text{src}}$ and $(X_{\text{tgt}}(1), \dots, X_{\text{tgt}}(b)) \sim \nu_{\text{tgt}}$ drawn respectively from the source and target distributions, and use these to define the *empirical Lagrangian*

$$\widehat{\mathcal{L}}(\mu, V) = \sum_{h=0}^H \int (c(x, y) + V_{h+1}(y) - V_h(x)) d\mu_h(x, y) + \frac{1}{b} \sum_{i=1}^b (V_0(X_{\text{src}}(i)) - V_{H+1}(X_{\text{tgt}}(i))).$$

Analogously, we define the *empirical dual function* as $\widehat{\mathcal{G}}(V) = \inf_{\mu \in \mathcal{S}^{H+1}} \widehat{\mathcal{L}}(\mu, V)$. Clearly, both of these are unbiased estimators of their population counterparts \mathcal{L} and \mathcal{G} , and thus stochastic gradients of \mathcal{G} can be obtained by evaluating the gradients of $\widehat{\mathcal{G}}$.

Primal parametrization and update rule. Computing the empirical dual function $\widehat{\mathcal{G}}$ is a highly nontrivial task, given that it involves optimizing over the set of probability distributions \mathcal{S}^{H+1} . We propose to address this problem by a nonparametric approach known as *Wasserstein gradient descent* [3, 23, 45, 8]. Specifically, for each time index $h = 0, 1, \dots, H$, we set up a system of $2b$ particles to represent μ_h , with a pair of particles corresponding to each sample pair $(X_{\text{src}}(i), X_{\text{tgt}}(i))$ within the minibatch. Denoting the pair by $(X_h^-(i), X_h^+(i))$ corresponding to time h and particle i , the distribution $\widehat{\mu}_h$ is written as $\widehat{\mu}_h = \frac{1}{b} \sum_{i=1}^b \delta_{(X_h^-(i), X_h^+(i))}$ where δ_z is the Dirac measure centered at $z \in \mathbb{R}^{2d}$. Then, the locations of the particles are updated by gradient descent as

$$\begin{aligned} X_h^-(i) &\leftarrow X_h^-(i) - \eta (\nabla_x c(X_h^-(i), X_h^+(i)) - \nabla_x V_h(X_h^-(i))) \\ X_h^+(i) &\leftarrow X_h^+(i) - \eta (\nabla_y c(X_h^-(i), X_h^+(i)) + \nabla_x V_{h+1}(X_h^+(i))), \end{aligned} \quad (7)$$

where $\eta > 0$ is a positive stepsize parameter, and ∇_x and ∇_y respectively refer to differentiation of the cost function with respect to its first and second arguments. After sufficiently many update steps, the procedure returns a particle system which can be used to evaluate the gradient of the approximate dual function $\widehat{\mathcal{L}}(\widehat{\mu}, V_{\theta})$ with respect to θ as the average of the sample gradients for all $i = 1, 2, \dots, b$:

$$\begin{aligned} \Delta_{\theta}(i) &= (\nabla_{\theta} V_{\theta}(X_{\text{src}}(i), 0) - \nabla_{\theta} V_{\theta}(X_0^-(i), 0)) + (\nabla_{\theta} V_{\theta}(X_H^+(i), H+1) - \nabla_{\theta} V_{\theta}(X_{\text{tgt}}(i), H+1)) \\ &+ \sum_{h=1}^H (\nabla_{\theta} V_{\theta}(X_{h-1}^+(i), h) - \nabla_{\theta} V_{\theta}(X_h^-(i), h)). \end{aligned} \quad (8)$$

For the primal updates to succeed, it is greatly beneficial to design a good initialization of the particles. Inspired by the structure of the optimal solution μ^* established in Theorem 3.1, we thus first compute

Algorithm 1: Primal-dual VDT training

Input: Set of source and target data points $(X_{\text{src}}(i))_{i=1}^n, (X_{\text{tgt}}(i))_{i=1}^n$;**For** $t = 1, 2, \dots, T$, **repeat**1. Sample minibatch $B = (X_{\text{src}}(i), X_{\text{tgt}}(i))_{i=1}^b$ and initialize particles via Eq. (9);2. **Primal updates:** For $k = 1, \dots, K$, update particles via Eq. (7);3. **Dual update:** Compute stochastic gradients via Eq. (8) and update parameters as $\theta \leftarrow \theta + \gamma \Delta_\theta$;**Return:** value function V_θ ;

a coupling $(X_{\text{src}}^*(i), X_{\text{tgt}}^*(i))_{i=1}^b$ of the source and target points in the minibatch, and set up the initial particle positions for all $h = 0, 1, \dots, H - 1$ as

$$X_h^+(i) = X_{h+1}^-(i) = \frac{H+1-h}{H+1} \cdot X_{\text{src}}^*(i) + \frac{h}{H+1} \cdot X_{\text{tgt}}^*(i). \quad (9)$$

The edge cases are initialized as $X_0^-(i) = X_{\text{src}}^*(i)$ and $X_H^+(i) = X_{\text{tgt}}^*(i)$. It is easy to see the resulting initial particle cloud $\hat{\mu}$ satisfies the constraints of (LP). Additionally, if the minibatch samples are coupled according to an OT map, Theorem 3.1 implies that $\hat{\mu}$ minimizes the empirical primal function $\sup_V \hat{\mathcal{L}}(\cdot, V)$. Thus, this initialization is expected to be nearly perfect when V_θ is close to V^* , and the number of primal updates necessary for good performance can be very low.

The algorithm. Our algorithm for training VDT policies then arises from combining the elements described above. In each training iteration $t = 1, 2, \dots, T$, we sample a minibatch of source and target points, initialize the corresponding set of particles and perform a sequence of primal updates, and finally evaluate the gradient of the resulting approximation of the dual function. The method is shown in pseudocode form as Algorithm 1. We provide further implementation details in Appendix C.

3.3 Generative modeling by value-driven transport

The trained value function V_θ can be directly used for purposes of generative modeling: to generate samples from the target, one draws a sample point from the source ν_{src} and then iteratively applies the learned VDT policy using Eq. (6). We outline a few possible extensions to this procedure below.

Generation time scales. On top of the structural properties already established, we can also show that the optimal value function V^* satisfies a certain invariance property with respect to the time horizon H (see Appendix B.4). Specifically, fixing any *time scale* $k > 0$ and considering two different horizons H and H_k with

$H_k + 1 = k(H + 1)$, we have that the corresponding value functions $V^{*,H}$ and V^{*,H_k} are related as $V_h^{*,H}(x) = V_{h_k}^{*,H_k}(x)$ for each $h_k = kh$. This implies that a value function V learned at a fixed H can be used for generation at various time scales. In particular, setting H_{test} as the test-time horizon, one can use the policy $\pi(x) = x - \frac{1}{H_{\text{test}}+1} \nabla_x V(x)$ for generation. To take advantage of this, it is convenient to parametrize V_θ so that, instead of the absolute time index h , it takes the normalized index h/H as input. We state our generation procedure using this convention as Algorithm 2.

Algorithm 2: VDT prediction

Input: value function V_θ , test horizon H_{test} ;**Init:** draw source sample $X_0 \sim \nu_{\text{src}}$;**For** $h = 0, 1, \dots, H_{\text{test}}$, **repeat**

$$X_{h+1} = X_h - \frac{1}{H_{\text{test}}+1} \nabla_x V_\theta(X_h, h/H_{\text{test}});$$

Translation tasks and reverse generation. Since our problem formulation and training method is entirely symmetric with respect to the roles of ν_{tgt} and ν_{src} , the learned value function can be used for reverse generation: for generating samples from ν_{src} given samples from ν_{tgt} , one simply needs to flip the sign and time-direction⁴ of the gradient updates in Equation (6). Additionally, Algorithm 1 is also suitable for dealing with so-called *paired* translation tasks where there is a known coupling between the data sets used for training, by taking this coupling into account when forming the minibatches.

Conditional generation. Our framework can easily be adapted to the important setup of conditional generation, where each source and target point is augmented with a class label (or other supplementary information such as a well-chosen embedding of caption text). This additional information can be easily incorporated by passing it as an additional argument to the value function. The training and generation procedures are straightforward to update accordingly.

⁴In fact, this reverse-generation procedure can be immediately read out from Equation (5).

Dataset	Wasserstein-2 distance from target				Path energy			
	moons	scurve	8gaussians	moons-8gaussians	moons	scurve	8gaussians	moons-8gaussians
100 step VDT+	0.131±0.034	0.120±0.013	0.435±0.123	0.652 ±0.151	1.238 ±0.059	1.629±0.027	14.386±0.135	30.444 ±0.311
10 step VDT+	0.132 ±0.029	0.125±0.013	0.424±0.111	0.626 ±0.097	1.236 ±0.058	1.623±0.026	14.290±0.148	29.989±0.278
1 step VDT+	0.229 ±0.008	0.262±0.004	0.809±0.025	1.365±0.039	1.066 ±0.073	1.358 ±0.026	10.817 ±0.254	22.679 ±0.333
100 step VDT	0.219±0.086	0.208±0.016	0.547±0.120	1.205 ±0.125	2.416 ±0.096	3.051±0.084	17.799±0.328	73.001 ±2.228
10 step VDT	0.307±0.035	0.273±0.058	0.565±0.073	1.360 ±0.077	2.272 ±0.073	2.955 ±0.07	18.046±0.332	76.488 ±2.682
1 step VDT	1.497 ±0.046	1.803±0.048	4.152 ±0.099	6.498 ±0.058	1.154 ±0.061	0.82 ±0.036	0.419 ±0.072	43.230 ±4.396
SF ² M+	0.124±0.023	0.128±0.005	0.275±0.058	0.726±0.137	1.183±0.043	1.686±0.039	14.66±0.173	31.36±0.930
SF ² M	0.185±0.028	0.201±0.062	0.393±0.054	1.482±0.151	2.08 ±0.146	3.01±0.173	16.74±0.274	107.3±9.695
DSBM-IMF++	0.123±0.014	0.130±0.025	0.276±0.030	0.802±0.172	1.594±0.043	2.116±0.018	14.88±0.252	41.09±1.206
DSBM-IMF	0.144±0.024	0.145±0.037	0.338±0.091	0.838±0.098	1.580±0.036	2.092±0.053	14.81±0.255	41.00±1.495
OT-CFM+	0.130±0.016	0.144±0.028	0.303±0.043	0.601±0.027	1.216±0.01	1.675±0.019	14.88±0.389	30.47±0.300
RF	0.283±0.045	0.345±0.079	0.421±0.071	1.525±0.330	1.269±0.088	1.793±0.107	15.06±0.447	36.11±2.701
oracle	-	-	-	-	1.123±0.01	1.631±0.03	14.43±0.045	30.02±0.076

Table 1: Sampling quality as measured by Wasserstein-2 distance to target and path energy for the 2D experiments, mean ± 1 standard deviation over 5 repetitions. More details and results in Appendix D.1.

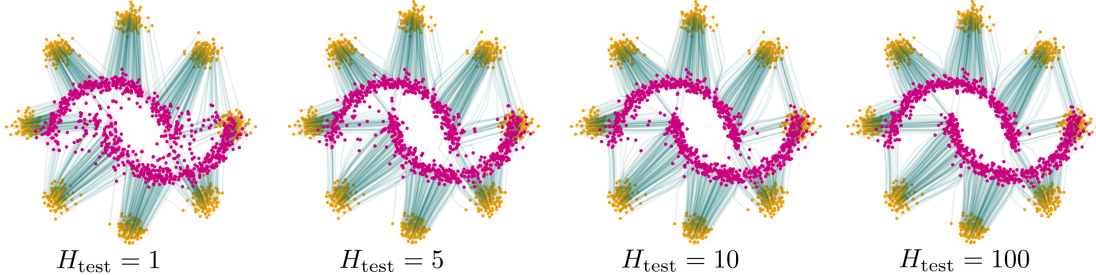


Figure 3: Few-step generation with a learned VDT model.

4 Experiments

We perform a range of numerical experiments to study the performance of our algorithm, and provide more insight about the properties of VDT policies. Instead of attempting to solve the most challenging generative modeling tasks (where competing methods have serious advantage due to the years of collective engineering experience they have benefited from), we aim to show that our method performs comparably with the best well-known methods in small-scale settings where thorough benchmarking of the methods themselves is possible. We also provide some early evidence that our method can achieve nontrivial behavior in large-scale data sets as well. Along the way, we highlight a few unique features of our methodology that might make it a desirable alternative to other frameworks.

4.1 2D experiments

We first evaluate our method in a range of 2D benchmark experiments inspired by Tong et al. [57, 58], also used by Shi et al. [51]. In our table, we reuse the figures reported by Tong et al. [58]. In most experiments, we set the source distribution as a standard Gaussian and vary the target distribution among three synthetic data sets (called “moons”, “scurve”, “8gauss”). In the last experiment, we set the source and target distributions as samples from the “moons” and “8gauss” data sets. We report an estimate of the Wasserstein-2 distance⁵ between the target and the generated distributions, as well as the “path energy” defined as $\sum_{h=0}^H c(X_h, X_{h+1})$ for each sample path. Since the path energy should approach the squared Wasserstein-2 distance for optimal transport paths, we also report estimates of this quantity in the last row of the table. For our own method, we report performance for two different particle-initialization schemes (naïve and OT, the latter version marked as “VDT+”), and various choices of prediction horizon H_{test} . We observe that using an OT map for particle initialization greatly improves generation quality, leading to reasonable accuracy already after a single generation step. Notably, the results for $H_{\text{test}} = 10$ and $H_{\text{test}} = H = 100$ are nearly identical, thus showing that one can gain a tenfold speedup in prediction time without having to make compromises about sample quality. Figure 3 illustrates the quality of few-step generation in the same setup. Complete details and more results are provided in Appendix D.1.

4.2 Experiments on MNIST

We next showcase the flexibility of the VDT framework by evaluating it on three common generative modeling tasks on the classic MNIST data set [27]. A more complete description of the experimental setups and more experiments are reported in Appendix D.2.

⁵For this comparison, we omit the $\frac{1}{2}$ factor featured in our definitions.

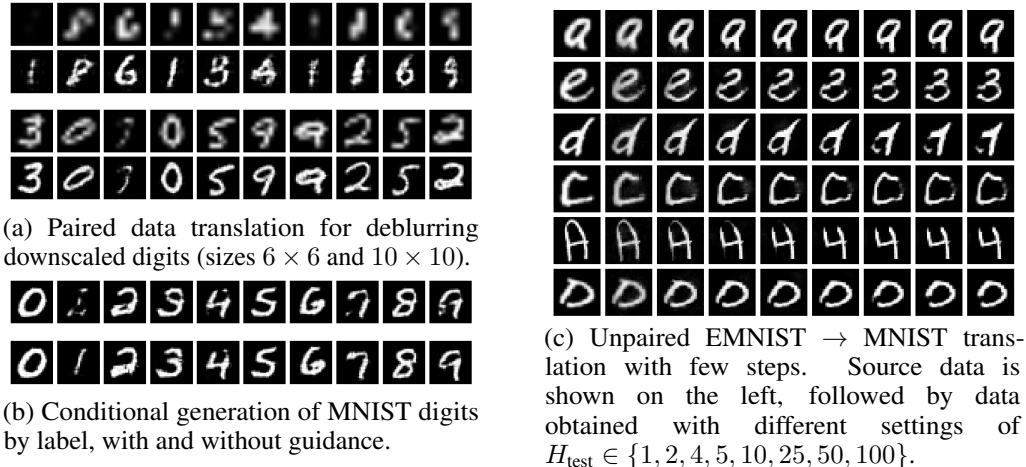


Figure 4: Experiments on MNIST: conditional generation and data translation.

Paired deblurring. The first task we consider is to deblur corrupted MNIST images. We downsample the original 28×28 MNIST images to dimension $m \times m$ and linearly upsample them back to the original full dimension. The resulting blurred image $S(i)$ is paired with its original counterpart $T(i)$ during VDT training. We train a model for $m = 6, 10, 14$ each and evaluate the result on a holdout set of unseen blurred MNIST images. As shown in Fig. 4a, the VDT policies are indeed able to reconstruct the clean image even after rather severe blurring.

Unpaired letter to digit translation. We next consider a task without naturally available pairings, namely the one of translating handwritten letters ('a'-'e' and 'A'-'E' from EMNIST [10]) to handwritten digits (0-9 from MNIST). We train a VDT model on unpaired minibatches of letters and digits, and show the results obtained on a holdout set by the few-step generation process for various choices of H_{test} in Figure 4c. While the sharpness of the generated digits could likely be improved through heavier training, they clearly exhibit the desired resemblance of the source letters, demonstrating that our algorithm can learn a nontrivial relation between the domains without explicit supervision. Additionally, we observe a similar test-time speedup achieved by few-step generation with $H_{\text{test}} = 10$, a factor 10 improvement over the training horizon $H = 100$.

Conditional image generation and guidance. Finally, we study the setup of conditional generation of MNIST digits. For this task, we augment our algorithm by concatenating the class label to the input of the parameterized value function and train it using the same methodology as for the other experiments. More importantly, an equally simple modification to the VDT training and inference procedure allows us to incorporate *classifier-free guidance* (CFG) [20], originally proposed for improving conditional generation quality of diffusion models. We provide more details in Appendix D.2. The results indicate that CFG affects the generation quality in the same way as it does for diffusion models: we obtain enhanced image quality at the expense of smaller sample diversity.

5 Limitations and outlook

Our new framework contributes to the already very busy research area of generative modeling. In many respects, our approach significantly departs from the mainstream within this area—we review the most notable similarities and differences in Appendix A. Besides holding strong promises for the future, this novelty also means that our results come with severe limitations. The most obvious of these is that, since our primal-dual algorithm for computing value functions is entirely new in this context, there are no available best practices that we could adapt in our implementation. Lacking such foundations to build on, we have not yet been able to scale the method to meaningfully attack the most challenging generative modeling tasks. We are confident that further experimentation will reveal better ways to tune our method so that it can reach its full potential, or to identify better algorithmic ideas to solve the linear program at the heart of our formulation. Indeed, we strongly believe that our methodology has significant conceptual advantages that can be turned into practical advantages once the training methodology we propose here is sufficiently refined, which is a challenge that we invite the reader to address in future work.

Acknowledgments and Disclosure of Funding

The authors thank the following colleagues for insightful discussions at various stages of working on this project: Lorenzo Croissant, Niao He, Gabriel Peyré, Anabel Pichardo, and Tina Sikharulidze. Additionally, the authors would like to thank Javier Segovia-Aguas, Anders Jonsson, and Vicenç Gómez for their advice and support on accessing the new UPF GPU cluster “Correfoc”. G. Neu was supported by the European Research Council (ERC) under the European Union’s Horizon 2020 research and innovation programme (Grant agreement No. 950180). Part of this research was performed while A. Müller was visiting the Institute for Mathematical and Statistical Innovation (IMSI), which is supported by the National Science Foundation (Grant No. DMS-2425650). P. Moreno-Muñoz was supported by “La Caixa” Banking Foundation through the Junior Leader Postdoctoral Fellowship Programme (Grant agreement ID code. LCF/BQ/PI24/12040025).

References

- [1] Michael S. Albergo and Eric Vanden-Eijnden. Building normalizing flows with stochastic interpolants. In *The Eleventh International Conference on Learning Representations*, 2023.
- [2] Michael S. Albergo, Nicholas M. Boffi, and Eric Vanden-Eijnden. Stochastic interpolants: A unifying framework for flows and diffusions. *Journal of Machine Learning Research*, 26(209): 1–80, 2025.
- [3] Luigi Ambrosio, Nicola Gigli, and Giuseppe Savaré. *Gradient flows: in metric spaces and in the space of probability measures*. Springer, 2005.
- [4] Joan Bas-Serrano, Sebastian Curi, Andreas Krause, and Gergely Neu. Logistic Q-learning. In *AI & Statistics*, pages 3610–3618, 2021.
- [5] Richard E. Bellman. *Dynamic Programming*. Princeton University Press, Princeton, New Jersey, 1957.
- [6] Jean-David Benamou and Yann Brenier. A computational fluid mechanics solution to the Monge–Kantorovich mass transfer problem. *Numerische Mathematik*, 84(3):375–393, 2000.
- [7] Dimitri P. Bertsekas. *Dynamic Programming and Optimal Control*, volume 1. Athena Scientific, Belmont, MA, 3 edition, 2007.
- [8] Luiz F. Chamon, Mohammad R. Karimi, and Anna Korba. Constrained sampling with primal-dual Langevin monte carlo. *Advances in Neural Information Processing Systems*, 37:29285–29323, 2024.
- [9] Ricky TQ Chen, Yulia Rubanova, Jesse Bettencourt, and David K Duvenaud. Neural ordinary differential equations. *Advances in neural information processing systems*, 31, 2018.
- [10] Gregory Cohen, Saeed Afshar, Jonathan Tapson, and Andre Van Schaik. Emnist: Extending mnist to handwritten letters. In *2017 international joint conference on neural networks (IJCNN)*, pages 2921–2926. IEEE, 2017.
- [11] Valentin De Bortoli, James Thornton, Jeremy Heng, and Arnaud Doucet. Diffusion Schrödinger bridge with applications to score-based generative modeling. *Advances in neural information processing systems*, 34:17695–17709, 2021.
- [12] Valentin De Bortoli, Iryna Korshunova, Andriy Mnih, and Arnaud Doucet. Schrödinger bridge flow for unpaired data translation. *Advances in Neural Information Processing Systems*, 37: 103384–103441, 2024.
- [13] Daniela P. de Farias and Benjamin Van Roy. The linear programming approach to approximate dynamic programming. *Operations Research*, 51(6):850–865, 2003.
- [14] Guy de Ghellinck. Les problèmes de décisions séquentielles. *Cahiers du Centre d’Études de Recherche Opérationnelle*, 2:161–179, 1960.
- [15] Eric V. Denardo. On linear programming in a Markov decision problem. *Management Science*, 16(5):281–288, 1970.

- [16] Francois d’Epenoux. A probabilistic production and inventory problem. *Management Science*, 10(1):98–108, 1963.
- [17] Prafulla Dhariwal and Alexander Nichol. Diffusion models beat gans on image synthesis. *Advances in neural information processing systems*, 34:8780–8794, 2021.
- [18] Nikita Gushchin, Sergei Kholkin, Evgeny Burnaev, and Alexander Korotin. Light and optimal schrödinger bridge matching. In *Forty-first International Conference on Machine Learning (ICML)*, 2024.
- [19] Nikita Gushchin, Daniil Selikhanovych, Sergei Kholkin, Evgeny Burnaev, and Alexander Korotin. Adversarial Schrödinger bridge matching. *Advances in Neural Information Processing Systems*, 37:89612–89651, 2024.
- [20] Jonathan Ho and Tim Salimans. Classifier-free diffusion guidance. *arXiv preprint arXiv:2207.12598*, 2022.
- [21] Jonathan Ho, Ajay Jain, and Pieter Abbeel. Denoising diffusion probabilistic models. *Advances in neural information processing systems*, 33:6840–6851, 2020.
- [22] Ronald A. Howard. *Dynamic Programming and Markov Processes*. The MIT Press, Cambridge, MA, 1960.
- [23] Richard Jordan, David Kinderlehrer, and Felix Otto. The variational formulation of the fokker-planck equation. *SIAM journal on mathematical analysis*, 29(1):1–17, 1998.
- [24] Tero Karras, Miika Aittala, Timo Aila, and Samuli Laine. Elucidating the design space of diffusion-based generative models. *Advances in neural information processing systems*, 35: 26565–26577, 2022.
- [25] Diederik P. Kingma and Jimmy Ba. Adam: A method for stochastic optimization. In *International Conference on Learning Representations (ICLR)*, 2015.
- [26] Chieh-Hsin Lai, Yang Song, Dongjun Kim, Yuki Mitsufuji, and Stefano Ermon. The principles of diffusion models. *arXiv preprint arXiv:2510.21890*, 2025.
- [27] Yann LeCun and Corinna Cortes. The MNIST database of handwritten digits. <http://yann.lecun.com/exdb/mnist/>.
- [28] Yaron Lipman, Ricky T. Q. Chen, Heli Ben-Hamu, Maximilian Nickel, and Matthew Le. Flow matching for generative modeling. In *The Eleventh International Conference on Learning Representations*, 2023.
- [29] Yaron Lipman, Marton Havasi, Peter Holderrieth, Neta Shaul, Matt Le, Brian Karrer, Ricky T.Q. Chen, David Lopez-Paz, Heli Ben-Hamu, and Itai Gat. Flow matching guide and code. *arXiv preprint arXiv:2412.06264*, 2024.
- [30] Guan-Horng Liu, Arash Vahdat, De-An Huang, Evangelos A. Theodorou, Weili Nie, and Anima Anandkumar. I2sb: image-to-image schrödinger bridge. In *Proceedings of the 40th International Conference on Machine Learning*, pages 22042–22062, 2023.
- [31] Qiang Liu. Rectified flow: A marginal preserving approach to optimal transport. *arXiv preprint arXiv:2209.14577*, 2022.
- [32] Xingchao Liu, Chengyue Gong, and Qiang Liu. Flow straight and fast: Learning to generate and transfer data with rectified flow. In *The Eleventh International Conference on Learning Representations (ICLR)*, 2023.
- [33] Fan Lu, Prashant G. Mehta, Sean P. Meyn, and Gergely Neu. Convex q-learning. In *2021 American Control Conference (ACC)*, pages 4749–4756. IEEE, 2021.
- [34] Alan S. Manne. Linear programming and sequential decisions. *Management Science*, 6(3): 259–267, 1960.

- [35] Robert J. McCann. A convexity principle for interacting gases. *Advances in mathematics*, 128 (1):153–179, 1997.
- [36] Kirill Neklyudov, Rob Brekelmans, Daniel Severo, and Alireza Makhzani. Action matching: Learning stochastic dynamics from samples. In *International conference on machine learning*, pages 25858–25889, 2023.
- [37] Gergely Neu and Nneka Okolo. Offline rl via feature-occupancy gradient ascent. In *International Conference on Artificial Intelligence and Statistics*, pages 3637–3645, 2025.
- [38] Gergely Neu, Anders Jonsson, and Vicenç Gómez. A unified view of entropy-regularized Markov decision processes. *arXiv preprint arXiv:1705.07798*, 2017.
- [39] Alexander Quinn Nichol and Prafulla Dhariwal. Improved denoising diffusion probabilistic models. In *International conference on machine learning*, pages 8162–8171, 2021.
- [40] F. Pedregosa, G. Varoquaux, A. Gramfort, V. Michel, B. Thirion, O. Grisel, M. Blondel, P. Prettenhofer, R. Weiss, V. Dubourg, J. Vanderplas, A. Passos, D. Cournapeau, M. Brucher, M. Perrot, and E. Duchesnay. Scikit-learn: Machine learning in Python. *Journal of Machine Learning Research*, 12:2825–2830, 2011.
- [41] Gabriel Peyré. Optimal and diffusion transports in machine learning. *arXiv preprint arXiv:2512.06797*, 2025.
- [42] Gabriel Peyré. Optimal transport for machine learners. *arXiv preprint arXiv:2505.06589*, 2025.
- [43] Martin L. Puterman. *Markov Decision Processes: Discrete Stochastic Dynamic Programming*. Wiley-Interscience, April 1994.
- [44] Danilo Rezende and Shakir Mohamed. Variational inference with normalizing flows. In *International conference on machine learning*, pages 1530–1538, 2015.
- [45] Adil Salim, Anna Korba, and Giulia Luise. The wasserstein proximal gradient algorithm. *Advances in Neural Information Processing Systems*, 33:12356–12366, 2020.
- [46] Filippo Santambrogio. *Optimal Transport for Applied Mathematicians: Calculus of Variations, PDEs, and Modeling*. Progress in Nonlinear Differential Equations and Their Applications. Birkhäuser Cham, 2015.
- [47] Filippo Santambrogio. L_1 and L_∞ theory. In *Optimal Transport for Applied Mathematicians: Calculus of Variations, PDEs, and Modeling*, pages 87–119. Springer, 2015.
- [48] Erwin Schrödinger. Über die Umkehrung der Naturgesetze. *Sitzungsberichte der Preußischen Akademie der Wissenschaften. Physikalisch-mathematische Klasse*, pages 144–153, 1931.
- [49] Paul J. Schweitzer and Abraham Seidman. Generalized polynomial approximations in Markovian decision processes. *J. of Math. Anal. and Appl.*, 110:568–582, 1985.
- [50] Alexander Shapiro. On duality theory of conic linear problems. *Nonconvex Optimization and its Applications*, 57:135–155, 2001.
- [51] Yuyang Shi, Valentin De Bortoli, Andrew Campbell, and Arnaud Doucet. Diffusion Schrödinger bridge matching. *Advances in neural information processing systems*, 36:62183–62223, 2023.
- [52] Jascha Sohl-Dickstein, Eric Weiss, Niru Maheswaranathan, and Surya Ganguli. Deep unsupervised learning using nonequilibrium thermodynamics. In *International conference on machine learning*, pages 2256–2265, 2015.
- [53] Jiaming Song, Chenlin Meng, and Stefano Ermon. Denoising diffusion implicit models. In *International Conference on Learning Representations*, 2021.
- [54] Yang Song, Jascha Sohl-Dickstein, Diederik P Kingma, Abhishek Kumar, Stefano Ermon, and Ben Poole. Score-based generative modeling through stochastic differential equations. *arXiv preprint arXiv:2011.13456*, 2020.

- [55] Richard S. Sutton and Andrew G. Barto. *Reinforcement Learning: An Introduction (second edition)*. online draft, 2018.
- [56] Matthew Thorpe. Introduction to optimal transport.
- [57] Alexander Tong, Kilian Fatras, Nikolay Malkin, Guillaume Hugué, Yanlei Zhang, Jarrid Rector-Brooks, Guy Wolf, and Yoshua Bengio. Improving and generalizing flow-based generative models with minibatch optimal transport. *Transactions on Machine Learning Research*, 2024.
- [58] Alexander Tong, Nikolay Malkin, Kilian Fatras, Lazar Atanackovic, Yanlei Zhang, Guillaume Hugué, Guy Wolf, and Yoshua Bengio. Simulation-free schrödinger bridges via score and flow matching. In *International Conference on Artificial Intelligence and Statistics*, pages 1279–1287, 2024.
- [59] Cédric Villani. *Topics in optimal transportation*, volume 58. American Mathematical Soc., 2003.
- [60] Pauli Virtanen, Ralf Gommers, Travis E Oliphant, Matt Haberland, Tyler Reddy, David Cournapeau, Evgeni Burovski, Pearu Peterson, Warren Weckesser, Jonathan Bright, et al. Scipy 1.0: fundamental algorithms for scientific computing in python. *Nature methods*, 17(3):261–272, 2020.
- [61] Max Welling and Yee Whye Teh. Bayesian learning via stochastic gradient langevin dynamics. In *Proceedings of the 28th international conference on machine learning (ICML-11)*, pages 681–688, 2011.
- [62] Ling Yang, Zhilong Zhang, Yang Song, Shenda Hong, Runsheng Xu, Yue Zhao, Wentao Zhang, Bin Cui, and Ming-Hsuan Yang. Diffusion models: A comprehensive survey of methods and applications. *ACM computing surveys*, 56(4):1–39, 2023.

Appendix

Contents

A Related work	14
B Discrete-time dynamic optimal transport	15
B.1 Definitions of OT problems	15
B.2 Basic properties of the OT problems	16
B.3 Value functions and the Bellman equations	19
B.4 Time scaling	22
C Further implementation details	24
C.1 Details of VDT training	24
C.2 Details of VDT prediction	25
D Experiments	25
D.1 2D experiments	26
D.2 MNIST experiments	27

A Related work

Our work fits into an already rich literature on formulating and solving generative modeling problems using tools of optimal transport. We review the most relevant previous work here, and refer the interested reader to one of the numerous recent surveys for a more complete treatment (some good examples being [29, 26]).

The idea of formulating generative modeling as an iterative process has been brought to the forefront of machine-learning research by works such as Rezende and Mohamed [44], Sohl-Dickstein et al. [52] and Chen et al. [9]. The ensuing literature came to be dominated by continuous-time formulations, whereby generation is regarded as a continuous-time process where initial samples drawn from a source distribution are pushed forward along solution paths of ordinary differential equations (ODEs) or stochastic differential equations (SDEs). Common ideas for training such continuous-time models include learning time-reversals of processes that gradually transform clean data into noise [52, 21, 54, 53, 17, 39, 24, 62] and fitting neural networks to fixed interpolations of source and target data sets [28, 31, 32, 57, 1, 36, 29, 2]. These approaches make use of tools of continuous-time mathematics (change-of-variable formulas, Fokker–Planck equations, etc.) and probabilistic modeling (likelihood-based objectives, score-based denoising, etc.), which are all very distinct from the tools we employ in the present paper. We provide a brief comparison with the most relevant past works below.

Flow-based models. Among flow-based models, a notable work we wish to highlight is the conditional flow matching (CFM) framework of Tong et al. [57]. At a high level, CFM aims at learning a transport map by fitting a vector field to minibatch estimates of the OT plan connecting the source and target distributions. While the idea of using minibatch estimates of the OT map also appears in our algorithm, there is a major difference in how the two methods make use of it: while CFM tries to merely lift the (possibly heavily biased) minibatch OT map to the entire state space, our method only uses it as initialization for the primal updates. During training, our algorithm keeps moving toward the true OT map over the entire data set (up to optimization and approximation errors), without suffering the consequences of the possible bias due to using small minibatches. Indeed, recall that an ideal implementation of our method will update the value-function parameters according to unbiased gradient estimates of the dual function, thus converging towards its maximizer—irrespective of the minibatch size or the initialization.

Another popular method within this family that we would like to mention is the rectified flow algorithm of Liu [31], Liu et al. [32]. Rectified flow models aim to approximate OT maps by iteratively refining a sequence of flow models: first, fit a flow model to i.i.d. samples from the true source and target distributions, then use the model to generate fresh, *coupled* samples from the learned model, fit a new model to this, and iterate. Under ideal conditions, this method can be shown to converge to an OT map, the error accumulation resulting from training each subsequent model

on the outputs of the previous model (without using any of the original samples) can be significant, which limits the applicability of this method for computing OT plans. A version of this method called c -rectified flow [31] aims at establishing a more direct link with the dynamic OT solution path by parametrizing the learned vector field as a gradient map of a scalar function (which is the form suggested by the Benamou–Brenier theorem). While this idea is attractive, it makes for a rather impractical method as it requires evaluating second derivatives of neural networks during training. In contrast, our method natively takes into account the structure of the optimal policy and optimizes estimates of the value function (a.k.a., the potential function).

Schrödinger bridges. Another important class of generative modeling tools make use of the concept of *Schrödinger bridges* (SB), defined as stochastic processes $(X_t)_{t \in [0,1]}$ with marginals $\text{Law}(X_0) = \nu_{\text{src}}$, $\text{Law}(X_1) = \nu_{\text{tgt}}$ and minimal relative entropy to a fixed reference process. Schrödinger bridges are closely linked with an entropy-regularized version of the Kantorovich OT problem (often called “entropic OT”, EOT), in a way analogous to the relation between dynamic and static OT (which we discussed in some detail in Section 2). Taking advantage of the many beautiful mathematical results about entropic OT, several successful generative models have been developed for approximating Schrödinger bridges [11, 51, 58, 30, 18, 19, 12]. While, like dynamic OT solution paths, Schrödinger bridges can also be succinctly parametrized by a single scalar-valued potential function (analogous to our value function), we are not aware of any method that utilizes this fact as straightforwardly as our method does. Indeed, SB-based methods typically feature multiple neural networks for parametrizing the control drifts (often separately in both time directions) and the dual variables for enforcing the source and target constraints, and use a variety of ideas from score-based generative modeling and flow matching during training. While these methods achieve outstanding empirical performance for a range of generative modeling tasks, the connection between their training methodologies and their core problem formulation is arguably often quite loose—making this a fruitful area of research with several interesting open problems.

B Discrete-time dynamic optimal transport

In this section, we provide a complete treatment of the discrete-time dynamic OT problem that our method is based on. To keep this section self-contained and easy to read, we will repeat some content already covered in the main text.

B.1 Definitions of OT problems

Definitions. Let $\nu_{\text{src}}, \nu_{\text{tgt}}$ be probability measures on \mathbb{R}^d . For probability measures γ over $\mathbb{R}^d \times \mathbb{R}^d$, consider the space of all (“marginal-preserving”) *couplings*

$$\Gamma(\nu_{\text{src}}, \nu_{\text{tgt}}) = \{\gamma \in \mathcal{S} \mid \mathcal{B}_{\#}\gamma = \nu_{\text{src}} \wedge \mathcal{F}_{\#}\gamma = \nu_{\text{tgt}}\}.$$

Consider the *Kantorovich problem*

$$\mathcal{W}_2^2(\nu_{\text{src}}, \nu_{\text{tgt}}) = \min_{\gamma \in \Gamma(\nu_{\text{src}}, \nu_{\text{tgt}})} \frac{1}{2} \int \|x - y\|^2 d\gamma(x, y). \quad (10)$$

If $\nu_{\text{src}}, \nu_{\text{tgt}}$ have densities $\rho_{\text{src}}, \rho_{\text{tgt}}$, this problem is known to admit the unique minimizer $\gamma^* = (\text{id}, M^*)_{\#}\nu_{\text{src}}$, where M^* is the unique minimizer of the *Monge problem*

$$\min_{\substack{M: \mathbb{R}^d \rightarrow \mathbb{R}^d \\ M_{\#}\nu_{\text{src}} = \nu_{\text{tgt}}}} \frac{1}{2} \int \|M(x) - x\|^2 d\nu_{\text{src}}(x), \quad (11)$$

and the optimal values of the programs coincide.

In analogy to the continuous-time dynamic Benamou–Brenier formulation of OT [6], we define the *discrete time dynamic OT problem* as follows. We consider a discrete-time stochastic control problem, where a sequence of states are generated recursively over a sequence of discrete *time steps* $h = 0, 1, \dots, H$ (where H is called the *horizon*). The initial state X_0 is drawn from the source distribution ν_{src} , and each consecutive state X_1, X_2, \dots, X_{H+1} is selected according to a *control policy* π that maps each state X_h to the next state as $X_{h+1} = \pi_h(X_h)$. The control cost associated with each state transition is $c(X_h, X_{h+1}) = \frac{H+1}{2} \|X_h - X_{h+1}\|^2$. In general, we will consider non-stationary policies represented as the collection of deterministic maps $\pi = \{\pi_h : \mathbb{R}^d \rightarrow \mathbb{R}^d\}_{h=0}^H$. A policy is called *feasible* if the law of the final state X_{H+1} generated by the above process matches

the target distribution ($\text{Law}(X_{H+1}) = \nu_{\text{tgt}}$), and we denote the set of feasible control policies by $\Pi(\nu_{\text{src}}, \nu_{\text{tgt}})$. Letting $\mathbb{E}_\pi[\cdot]$ stand for the expectation operator under the joint distribution of state sequences generated by π , we then set up our objective as

$$\mathcal{W}_{\text{dyn-M},2}^2(\nu_{\text{src}}, \nu_{\text{tgt}}) = \min_{\pi \in \Pi(\nu_{\text{src}}, \nu_{\text{tgt}})} \frac{H+1}{2} \sum_{h=0}^H \mathbb{E}_\pi \left[\|X_{h+1} - X_h\|^2 \right]. \quad (12)$$

We reformulate this optimization problem using the concept of *occupancy measures*, borrowed from the literature on optimal control in discrete-time Markov decision processes (see, e.g., Chapter 6.9 in Puterman [43]). The occupancy measure associated with a control policy π is the collection of joint distributions $\mu^\pi = \{\mu_h^\pi \in \Delta_{\mathbb{R}^d \times \mathbb{R}^d}\}_{h=0}^H$ over the state space, with $\mu_h^\pi = \mathbb{P}_\pi[(X_h, X_{h+1}) \in \cdot]$ corresponding to the distribution of the state pair X_h, X_{h+1} generated by policy π under the discrete-time control process described above. As is well-known in the context of Markov decision processes, the set of all valid occupancy measures that can be induced by control policies is uniquely characterized by a set of linear constraints. Adapting these results to our needs, we formulate our optimal control problem as the following linear program (LP):

$$\begin{aligned} \mathcal{W}_{\text{dyn-K},2}^2(\nu_{\text{src}}, \nu_{\text{tgt}}) &= \min_{\mu \in \mathcal{S}^{H+1}} \frac{H+1}{2} \sum_{h=0}^H \int \|x - y\|^2 d\mu_h(x, y) \\ \text{s.t.} \quad \nu_{\text{src}} &= \mathcal{B}_\# \mu_0 \\ \mathcal{F}_\# \mu_h &= \mathcal{B}_\# \mu_{h+1} \quad (\forall h \in \{0, \dots, H-1\}) \\ \mathcal{F}_\# \mu_H &= \nu_{\text{tgt}} \end{aligned} \quad (\text{Primal LP})$$

To distinguish between the two formulations, we will refer to the first as the *Monge-type dynamic OT* problem, and the second one as the *Kantorovich-type dynamic OT problem*, which naming convention is justified by noticing that the first problem reduces to the Monge-type OT problem (11) and the second to the Kantorovich-type problem (10). Throughout the appendix, we will refer to this LP as the *primal LP*, which otherwise coincides with (LP) shown in the main text.

B.2 Basic properties of the OT problems

We first establish that the Kantorovich problem (10) is equivalent to the Kantorovich-type dynamic OT problem in (Primal LP):

Theorem B.1. *We have*

$$\mathcal{W}_{\text{dyn-K},2}^2(\nu_{\text{src}}, \nu_{\text{tgt}}) = \mathcal{W}_2^2(\nu_{\text{src}}, \nu_{\text{tgt}}).$$

Moreover, if γ^* is optimal for Eq. (2), let $(X_0, X_{H+1}) \sim \gamma^*$ and $X_h = X_0 + \frac{h}{H+1}(X_{H+1} - X_0)$. Then, the laws μ_h^* of (X_h, X_{h+1}) form an optimal solution μ^* for (Primal LP).

Proof. We start by showing $\mathcal{W}_{\text{dyn-K},2}^2(\nu_{\text{src}}, \nu_{\text{tgt}}) = \mathcal{W}_2^2(\nu_{\text{src}}, \nu_{\text{tgt}})$. To this end, let $\mu \in \mathcal{S}^{H+1}$ be feasible for (Primal LP). By inductively applying the gluing lemma (e.g., [56, Lemma 5.5]), we can pick a measure $\bar{\mu}$ over sequences in \mathcal{X}^{H+2} and random variables $Y = (Y_0, \dots, Y_{H+1}) \sim \bar{\mu}$ such that for all $h \in \{0, \dots, H\}$, $(Y_h, Y_{h+1}) \sim \mu_h$. Now the dynamic objective for this choice is

$$\begin{aligned} \frac{H+1}{2} \sum_{h=0}^H \int \|x - y\|^2 d\mu_h(x, y) &= \frac{(H+1)^2}{2} \mathbb{E} \left[\frac{1}{H+1} \sum_{h=0}^H \|Y_h - Y_{h+1}\|^2 \right] \\ &\geq \frac{(H+1)^2}{2} \mathbb{E} \left[\left\| \frac{1}{H+1} \sum_{h=0}^H (Y_h - Y_{h+1}) \right\|^2 \right] \quad (\text{by Jensen's}) \\ &= \frac{1}{2} \mathbb{E} \left[\|Y_0 - Y_{H+1}\|^2 \right] \\ &= \frac{1}{2} \int \|x - y\|^2 d\gamma(x, y), \end{aligned}$$

where in the last step γ is the law of (Y_0, Y_{H+1}) (formally obtained by marginalization of $\bar{\mu}$). It satisfies $\mathcal{B}_\# \gamma = \nu_{\text{src}}$ and $\mathcal{F}_\# \gamma = \nu_{\text{tgt}}$, so the above implies

$$\frac{H+1}{2} \sum_{h=0}^H \int \|x - y\|^2 d\mu_h(x, y) \geq \mathcal{W}_2^2(\nu_{\text{src}}, \nu_{\text{tgt}}).$$

Thus, we obtain that $\mathcal{W}_{\text{dyn-K},2}^2(\nu_{\text{src}}, \nu_{\text{tgt}}) \geq \mathcal{W}_2^2(\nu_{\text{src}}, \nu_{\text{tgt}})$ after taking the infimum over all feasible μ on the left-hand side.

Next, we show $\mathcal{W}_{\text{dyn-K},2}^2(\nu_{\text{src}}, \nu_{\text{tgt}}) \leq \mathcal{W}_2^2(\nu_{\text{src}}, \nu_{\text{tgt}})$ and the optimality of μ^* . Let $(X_0, X_{H+1}) \sim \gamma^*$ and take $X_h = X_0 + \frac{h}{H+1}(X_{H+1} - X_0)$ as in the theorem statement, with the associated marginal distributions denoted by $\mu_h^* = \text{law}(X_h, X_{h+1})$. It is immediate that μ^* respects all of the constraints in (Primal LP). Moreover, we have

$$\begin{aligned} \frac{H+1}{2} \sum_{h=0}^H \int \|x - y\|^2 d\mu_h^*(x, y) &= \mathbb{E} \left[\frac{H+1}{2} \sum_{h=0}^H \|X_h - X_{h+1}\|^2 \right] \\ &= \mathbb{E} \left[\frac{H+1}{2} \sum_{h=0}^H \left\| \frac{1}{H+1} (X_0 - X_{H+1}) \right\|^2 \right] \\ &= \frac{1}{2} \mathbb{E} \left[\|(X_0 - X_{H+1})\|^2 \right] \\ &= \frac{1}{2} \int \|x - y\|^2 d\gamma^*(x, y) \\ &= \mathcal{W}_2^2(\nu_{\text{src}}, \nu_{\text{tgt}}). \end{aligned}$$

This proves the claimed inequality. Together with the reverse inequality we have proved first, we can also see that in fact $\mathcal{W}_{\text{dyn-K},2}^2(\nu_{\text{src}}, \nu_{\text{tgt}})$ is equal to the value obtained by μ^* , which implies that it is an optimal solution for (Primal LP). \square

We remark that this proof is very similar to the original proof of the Benamou-Brenier formula but without the need of change of measure arguments, with the discrete-time flow constraints replacing the continuity equation. We discuss this relationship in more detail later in this section.

We next establish the connection to the Monge-type dynamic OT problem (12). More concretely, we can now show the existence of deterministic optimal policies under suitable conditions by leveraging the following standard result from static OT theory.

Lemma B.1 (Santambrogio [46], Lemma 4.23). *Let M^* be an optimal solution to the static Monge problem in (1) and $\gamma = (id, M^*)_{\#} \nu_{\text{src}}$. Let $t \in (0, 1)$ and $y \in \mathbb{R}^d$. Then, there is at most one pair $(x, z) \in \text{supp}(\gamma)$ such that $y = (1-t)x + tz$.*

This fact (originally due to McCann [35]) implies that the optimal interpolants of the static Monge problem do not cross, which leads to the following result.

Theorem B.2. *Suppose that the static Monge problem (1) admits a solution M^* . Then, the dynamic Monge-type problem in (12) admits a optimal solution π^* . Moreover, if M^* is unique on $\text{supp}(\nu_{\text{src}})$, then each π_h^* is uniquely defined on $\text{supp}((1-h/(H+1))id + h/(H+1)M^*)_{\#} \nu_{\text{src}}$ with an expression given by*

$$\pi_h^*(x_h) = s_h(x_h) + \frac{h+1}{H+1} (M^*(s_h(x_h)) - s_h(x_h)),$$

where $s_h(x_h) = \left[(1 - \frac{h}{H+1})id + \frac{h}{H+1}M^* \right]^{-1}(x_h)$.

Proof. We prove the two claims regarding existence and uniqueness of π^* below.

Existence. Consider π^* as in the theorem statement and let $x_0 \in \text{supp}(\nu_{\text{src}})$. Denote the interpolation map by $f_h(x) = (1 - h/(H+1))id + h/(H+1)M^*$. Note that $s_0(x_0) = x_0$ and thus $x_1 = \pi_0^*(x_0) = x_0 + 1/(H+1)(M^*(x_0) - x_0) = f_1(x_0) \in \text{supp}((f_1)_{\#} \nu_{\text{src}})$. Now, let us consider a fixed h and let $x_h = f_h(x_0)$. Then by Lemma B.1, s_h is well-defined and $s_h(x_h) = x_0$. Hence, $\pi_h^*(x_h) = x_0 + (h+1)/(H+1)(M^*(x_0) - x_0) = f_{h+1}(x_0)$. This shows inductively that for $x_0 \in \text{supp}(\nu_{\text{src}})$, the sequence given via $x_{h+1} = \pi_h^*(x_h)$ is well-defined and in fact satisfies $x_h = f_h(x_0)$ for all h . It follows that π^* is feasible for (12) since $\pi_H^* \circ \dots \circ \pi_0^* = M^*$ on $\text{supp}(\nu_{\text{src}})$. Moreover, the objective

is

$$\begin{aligned}\mathbb{E}_{\pi^*} \left[\frac{H+1}{2} \sum_{h=0}^H \|X_{h+1} - X_h\|^2 \right] &= \mathbb{E} \left[\frac{H+1}{2} \sum_{h=0}^H \left\| \frac{1}{H+1} (M^*(X_0) - X_0) \right\|^2 \right] \\ &= \frac{1}{2} \mathbb{E} \left[\|M^*(X_0) - X_0\|^2 \right] \\ &= \mathcal{W}_2^2(\nu_{\text{src}}, \nu_{\text{tgt}}).\end{aligned}$$

where we used that M^* realizes $\mathcal{W}_2^2(\nu_{\text{src}}, \nu_{\text{tgt}})$. On the other hand, introducing the shorthand notation $\bar{\pi}_h = \pi_h \circ \dots \circ \pi_0$, we can see that any feasible policy π must satisfy

$$\begin{aligned}\mathbb{E}_{\pi} \left[\frac{H+1}{2} \sum_{h=0}^H \|X_{h+1} - X_h\|^2 \right] &= \frac{(H+1)^2}{2} \mathbb{E} \left[\frac{1}{H+1} \sum_{h=0}^H \|\bar{\pi}_h(X_0) - \bar{\pi}_{h-1}(x_0)\|^2 \right] \\ &\geq \frac{(H+1)^2}{2} \mathbb{E} \left[\left\| \frac{1}{H+1} \sum_{h=0}^H (\bar{\pi}_h(X_0) - \bar{\pi}_{h-1}(X_0)) \right\|^2 \right] \quad (\text{by Jensen's inequality}) \\ &= \frac{1}{2} \mathbb{E} \left[\|X_0 - \pi_H \circ \dots \circ \pi_0(X_0)\|^2 \right] \\ &\geq \mathcal{W}_2^2(\nu_{\text{src}}, \nu_{\text{tgt}}),\end{aligned}$$

where in the final step we used that $\pi_H \circ \dots \circ \pi_0$ is feasible for (1) since π is feasible for (Primal LP) in the final step. This implies that π^* is indeed optimal for (Primal LP).

Uniqueness. If π is optimal, then (since Jensen's holds point-wise within the expectation), the above chain of inequalities shows that for any realization of x_0 and the induced sequence $x_{h+1} = \pi_h(x_h)$, we must have $x_{h+1} - x_h = x_1 - x_0$ for any h . Thus we have

$$\mathbb{E}_{\pi} \left[(H+1) \sum_{h=0}^H \|X_{h+1} - X_h\|^2 \right] = \mathbb{E} \left[\|X_0 - \pi_H \circ \dots \circ \pi_0(X_0)\|^2 \right].$$

Since π is feasible, this equals $\mathcal{W}_2^2(\nu_{\text{src}}, \nu_{\text{tgt}})$ if and only if $\pi_H \circ \dots \circ \pi_0$ is optimal for the static problem (1), and thus must satisfy $\pi_H \circ \dots \circ \pi_0 = M^*$ on $\text{supp}(\nu_{\text{src}})$. Since $x_{h+1} - x_h = x_1 - x_0$, it follows that $\pi_h(x_h) = \pi_h^*(x_h)$ on $\text{supp}((f_h)_{\#}\nu_{\text{src}})$. \square

Putting Theorems B.1 and B.2 together immediately implies that the Monge- and Kantorovich-type dynamic OT problems are equivalent. We state this formally and connect the solutions μ^* and π^* to each other explicitly below.

Corollary B.1. *Suppose that the static Monge problem (1) admits the unique (on $\text{supp}(\nu_{\text{src}})$) solution M^* . Let π^* be the optimal solution of the dynamic Monge-type problem (12). Then, μ^* given by $\mu_h^* = (\pi_{h-1}^* \circ \dots \circ \pi_0^*)_{\#}\nu_{\text{src}}$ (with the convention $\pi_{-1}^* \circ \dots \circ \pi_0^* = \text{id}$) is an optimal solution for the dynamic Kantorovich-type problem (Primal LP) and has the same value.*

Proof. Let μ^* be defined as in the statement. By construction, we have $\mathcal{B}_{\#}\mu_0^* = \text{id}_{\#}\nu_{\text{src}} = \nu_{\text{src}}$ and $\mathcal{F}_{\#}\mu_h^* = (\pi_h^* \circ \dots \circ \pi_0^*)_{\#}\nu_{\text{src}} = \mathcal{B}_{\#}\mu_{h+1}^*$, as well as $\mathcal{F}_{\#}\mu_H^* = (\pi_H^* \circ \dots \circ \pi_0^*)_{\#}\nu_{\text{src}} = \nu_{\text{tgt}}$. Thus, μ^* is feasible for (Primal LP).

Let $W(\mu^*)$ be the value of (Primal LP) for this μ^* . Now, let us consider the set of random variables defined recursively as $X_0 \sim \nu_{\text{src}}$ and $X_{h+1} = \pi_h^*(X_h)$ for each h . Then, the pair (X_h, X_{h+1}) is distributed as μ_h^* and hence the value $W(\mu^*)$ coincides with that of (Primal LP) for the optimal π^* . Hence, as seen in the proof of Theorem B.2, $M^* = \pi_H^* \circ \dots \circ \pi_0^*$ is optimal for the static Monge problem in Eq. (1) with value $W(\mu^*)$. The latter thus also equals the value of the static Kantorovich problem in Eq. (2). In turn, Theorem B.1 thus shows that the optimal value of the Kantorovich-style dynamic OT problem of (Primal LP) is indeed $W(\mu^*)$. Hence μ^* is optimal for (Primal LP). \square

Altogether, the results in this section prove the claims made in Theorem 3.1.

B.3 Value functions and the Bellman equations

In the following, we restrict the problem to the domains $\mathcal{M} = \mathcal{M}_{\geq 0}(\Omega \times \Omega)$ and $\mathcal{C}(\Omega)$ over a compact convex set $\Omega \subset \mathbb{R}^d$ rather than all of \mathbb{R}^d . That is, we assume that $\text{supp}(\nu_{\text{src}}), \text{supp}(\nu_{\text{tgt}}) \subset \Omega$. Then, all previous statements then hold analogously for the optimization problems over these domains, with the addition that the maps π^* in Theorem B.2 are continuous (see [47, Lemma 5.29]).⁶

We define the *Lagrangian* associated with the constrained optimization problem (Primal LP) as

$$\begin{aligned} \mathcal{L}(\mu, V) &= \frac{H+1}{2} \sum_{h=0}^H \int \|x-y\|^2 d\mu_h(x, y) + \int V_0(x) d(\nu_{\text{src}} - \mathcal{B}_{\#}\mu_0)(x) \\ &\quad + \sum_{h=1}^H \int V_h(x) d(\mathcal{F}_{\#}\mu_{h-1} - \mathcal{B}_{\#}\mu_h)(x) + \int V_{H+1}(x) d(\mathcal{F}_{\#}\mu_H - \nu_{\text{tgt}})(x) \\ &= \sum_{h=0}^H \int \left(\frac{H+1}{2} \|x-y\|^2 + V_{h+1}(y) - V_h(x) \right) d\mu_h(x, y) \\ &\quad + \int V_0(x) d\nu_{\text{src}}(x) - \int V_{H+1}(x) d\nu_{\text{tgt}}(x) \end{aligned}$$

and consider the (primal) Lagrangian formulation equivalent to the dynamic OT problem:

$$\mathcal{W}_{\text{dyn},2}^2(\nu_{\text{src}}, \nu_{\text{tgt}}) = \inf_{\mu \in \mathcal{M}^{H+1}} \sup_{V \in \mathcal{C}(\Omega)^{H+2}} \mathcal{L}(\mu, V). \quad (\text{P})$$

Note that we relaxed the condition on μ to unnormalized measures $\mu_h \in \mathcal{M} = \mathcal{M}_{\geq 0}(\Omega \times \Omega)$ since the feasibility set of the dynamic Kantorovich problem already ensures that μ is normalized. Indeed, notice that by the first marginal constraint, we have $1 = \nu_{\text{src}}(\Omega) = [\mathcal{B}_{\#}\mu_0](\Omega) = \mu_0(\mathcal{B}^{-1}(\Omega)) = \mu_0(\Omega \times \Omega)$. Inductively, if $1 = \mu_h(\Omega \times \Omega)$, using the flow constraint we have $1 = \mu_h(\Omega \times \Omega) = \mu_h(\mathcal{F}^{-1}(\Omega)) = [\mathcal{F}_{\#}\mu_h](\Omega) = [\mathcal{B}_{\#}\mu_{h+1}](\Omega) = \mu_{h+1}(\mathcal{B}^{-1}(\Omega)) = \mu_{h+1}(\Omega \times \Omega)$.

We can now consider the *dual* of this problem, defined as

$$\sup_{V \in \mathcal{C}(\Omega)^{H+2}} \inf_{\mu \in \mathcal{M}^{H+1}} \mathcal{L}(\mu, V), \quad (\text{D})$$

and show that it can be equivalently formulated as the *dual linear program* stated below.

Lemma B.2. *The dual problem in Eq. (D) is equivalent to*

$$\begin{aligned} \max_{V \in \mathcal{C}(\Omega)^{H+2}} \int V_0(x) d\nu_{\text{src}}(x) - \int V_{H+1}(x) d\nu_{\text{tgt}}(x) \\ \text{s.t.} \quad V_h(x) \leq \frac{H+1}{2} \|x-y\|^2 + V_{h+1}(y) \quad (\forall h \in 0, \dots, H \forall x, y \in \Omega). \end{aligned} \quad (\text{Dual LP})$$

This can be seen to be analogous to the classic dual LP for optimal control in Markov decision processes, with the difference that the objective involves the target measure as a new element (rather than merely the value V_0 averaged over an initial state distribution). The derivation of the dual LP is a special case of general conic LPs [50].

Proof of Lemma B.2. Writing the Lagrangian in its ‘‘adjoint’’ form, we have

$$\begin{aligned} \mathcal{L}(\mu, V) &= \sum_{h=0}^H \int \left(\frac{H+1}{2} \|x-y\|^2 + V_{h+1}(y) - V_h(x) \right) d\mu_h(x, y) \\ &\quad + \int V_0(x) d\nu_{\text{src}}(x) - \int V_{H+1}(x) d\nu_{\text{tgt}}(x). \end{aligned}$$

Clearly, we have $\inf_{\mu \in \mathcal{M}^{H+1}} \mathcal{L}(\mu, V) = -\infty$ whenever there is h and a set $A \subset \Omega \times \Omega$ of strictly positive Lebesgue measure such that $V_h(x) > \frac{H+1}{2} \|x-y\|^2 + V_{h+1}(y)$ for all $(x, y) \in A$. On the other hand, if this is not the case, then $\mathcal{L}(\mu, V) \geq \int V_0(x) d\nu_{\text{src}}(x) - \int V_{H+1}(x) d\nu_{\text{tgt}}(x)$ for all $\mu \in \mathcal{M}^{H+1}$, with equality holding for instance when all $\mu_h = 0$. Thus $\inf_{\mu \in \mathcal{M}^{H+1}} \mathcal{L}(\mu, V) = \int V_0(x) d\nu_{\text{src}}(x) - \int V_{H+1}(x) d\nu_{\text{tgt}}(x)$. Hence V is optimal for the dual problem (D) if and only if it solves the LP in the statement. \square

⁶This is needed to have measures and continuous functions to be properly paired spaces, and to establish duality.

Recall (e.g., from [42]) the *dual of the static OT problem* in Eq. (2) is given by

$$\begin{aligned} \max_{W_0, W_1 \in \mathcal{C}(\Omega)} & \int W_0(x) d\nu_{\text{src}}(x) - \int W_1(x) d\nu_{\text{tgt}}(x) \\ \text{s.t.} & \quad W_0(x) \leq \frac{1}{2} \|x - y\|^2 + W_1(y) \quad (\forall x, y \in \mathbb{R}^d). \end{aligned} \quad (13)$$

This is sometimes equivalently written as by directly setting $W_1 = -(W_0)^*$ to be the negative $\|\cdot\|^2$ -transform of $-W_0$ and optimizing only over W_0 . We now show that the dual of the dynamic OT problem is equivalent to the dual of the static problem, and then use this to establish strong duality.

Theorem B.3 (Equivalence to the Static Dual). *Let V^* be optimal for the dynamic dual problem (Dual LP). Then, $W_0 = V_0^*$ and $W_1 = V_{H+1}^*$ form an optimal solution for the static dual problem (13) and in particular the optimal values coincide.*

Proof. Feasibility: For any $x, y \in \mathbb{R}^d$, set $x_h = (1 - h/(H + 1))x + h/(H + 1)y$ (for $h = 0, \dots, H + 1$) and notice that

$$\begin{aligned} W_0(x) = V_0^*(x_0) & \leq \frac{H+1}{2} \|x_0 - x_1\|^2 + V_1^*(x_1) \\ & \leq \dots \\ & \leq \frac{H+1}{2} \sum_{h=0}^H \|x_h - x_{h+1}\|^2 + V_{H+1}^*(x_{H+1}) \\ & = \frac{H+1}{2} \sum_{h=0}^H \left\| \frac{1}{(H+1)}(x - y) \right\|^2 + V_{H+1}^*(x_{H+1}) \\ & = \frac{1}{2} \|x - y\|^2 + W_1(y), \end{aligned}$$

so (W_0, W_1) is feasible for the problem in Eq. (13).

Optimality: Assume by contradiction that W^* is optimal for the problem in Eq. (13) and satisfies

$$\begin{aligned} \int W_0^*(x) d\nu_{\text{src}}(x) - \int W_1^*(x) d\nu_{\text{tgt}}(x) & > \int W_0(x) d\nu_{\text{src}}(x) - \int W_1(x) d\nu_{\text{tgt}}(x) \\ & = \int V_0^*(x) d\nu_{\text{src}}(x) - \int V_{H+1}^*(x) d\nu_{\text{tgt}}(x). \end{aligned} \quad (14)$$

Let us proceed by defining the sequence $V'_{H+1} = W_1^*$ and $V'_h(x) = \min_{y \in \Omega} \left(\frac{H+1}{2} \|x - y\|^2 + V'_{h+1}(y) \right)$ inductively for $h = H, \dots, 0$. Clearly, V' is feasible for the dynamic dual problem (Dual LP). Moreover, by construction, for any $x_0 \in \mathbb{R}^d$ we have

$$\begin{aligned} V'_0(x_0) & = \min_{x_1} \left(\frac{H+1}{2} \|x_0 - x_1\|^2 + V'_1(x_1) \right) \\ & = \dots \\ & = \min_{x_1, \dots, x_{H+1}} \left(\frac{H+1}{2} \sum_{h=0}^H \|x_h - x_{h+1}\|^2 + V'_{H+1}(x_{H+1}) \right) \\ & \geq \min_{x_1, \dots, x_{H+1}} \left(\frac{(H+1)^2}{2} \left\| \frac{1}{H+1} \sum_{h=0}^H (x_h - x_{h+1}) \right\|^2 + V'_{H+1}(x_{H+1}) \right) \quad (\text{by Jensen's}) \\ & = \min_{x_{H+1}} \left(\frac{1}{2} \|x_0 - x_{H+1}\|^2 + W_1^*(x_{H+1}) \right). \end{aligned}$$

Now, when $x_0 \in \text{supp}(\nu_{\text{src}})$, we know that the right-hand side equals $W_0^*(x_0)$ [42]. Hence, we have $V'_0 \geq W_0$ (on $\text{supp}(\nu_{\text{src}})$) and $V'_{H+1} = W_1$. Thus, since V' is feasible for the dynamic dual and V^*

is optimal, we have

$$\begin{aligned} \int V_0^*(x) d\nu_{\text{src}}(x) - \int V_{H+1}^*(x) d\nu_{\text{tgt}}(x) &\geq \int V_0'(x) d\nu_{\text{src}}(x) - \int V_{H+1}'(x) d\nu_{\text{tgt}}(x) \\ &\geq \int W_0^*(x) d\nu_{\text{src}}(x) - \int W_1^*(x) d\nu_{\text{tgt}}(x), \end{aligned}$$

contradicting the inequality (14), thus proving our original claim. \square

We thus obtain that the dynamic OT problem inherits strong duality from the static OT problem.

Lemma B.3 (Strong duality). *The values of (Primal LP) and (Dual LP) coincide.*

Proof. Let OPT_P and OPT_D denote the optimal values of the static primal (Eq. (2)) and dual problems Eq. (13), respectively. By strong duality of the static problem [42], we have $\text{OPT}_P = \text{OPT}_D$. Further, let $\text{OPT}_P^{\text{dyn}}$ and $\text{OPT}_D^{\text{dyn}}$ denote the optimal values of the dynamic primal (Eq. (P)) and dual (Eq. (D)), respectively. By Theorem B.1, we have $\text{OPT}_P^{\text{dyn}} = \text{OPT}_P$. By Theorem B.3, we have $\text{OPT}_D^{\text{dyn}} = \text{OPT}_D$. Hence $\text{OPT}_P^{\text{dyn}} = \text{OPT}_D^{\text{dyn}}$. \square

By strong duality, we can now show that the dual program admits a dynamic programming interpretation, connecting it to the policies of the Monge-type dynamic OT problem.

Theorem B.4. [Theorem 3.2 in the main text] *Let μ^* be an optimal solution for (Primal LP) that corresponds to a deterministic policy π^* . Let V^* be an optimal solution for (Dual LP). Then for all h and for $(\pi_{h-1}^* \circ \dots \circ \pi_0^*)_{\#} \nu_{\text{src}}$ -almost all $x \in \Omega$, the optimal value dual variables and the optimal policy respectively satisfy*

$$\begin{aligned} V_h^*(x) &= \min_{y \in \Omega} \left(\frac{H+1}{2} \|x - y\|^2 + V_{h+1}^*(y) \right), \\ \pi_h^*(x) &= \arg \min_{y \in \Omega} \left(\frac{H+1}{2} \|x - y\|^2 + V_{h+1}^*(y) \right). \end{aligned}$$

Proof. For ease of notation, we define $\bar{\pi}_h = \pi_h^* \circ \dots \circ \pi_0^*$. By strong duality (Lemma B.3) and the fact that $(\bar{\pi}_H)_{\#} \nu_{\text{src}} = \nu_{\text{tgt}}$ by feasibility, we have

$$\begin{aligned} &\frac{H+1}{2} \sum_{h=0}^H \int \|\pi_h^*(x) - x\|^2 d(\bar{\pi}_{h-1} \# \nu_{\text{src}})(x) \\ &= \int V_0^*(x) d\nu_{\text{src}}(x) - \int V_{H+1}^*(x) d\nu_{\text{tgt}} \\ &= \int V_0^*(x) d\nu_{\text{src}}(x) - \int V_{H+1}^*(x) d((\bar{\pi}_H)_{\#} \nu_{\text{src}})(x) \\ &= \int (V_0^*(x) - V_{H+1}^*(\bar{\pi}_H(x))) d\nu_{\text{src}}(x) \\ &= \sum_{h=0}^H \int (V_h^*(\bar{\pi}_{h-1}(x)) - V_{h+1}^*(\pi_h^*(\bar{\pi}_{h-1}(x)))) d\nu_{\text{src}}(x) \\ &= \sum_{h=0}^H \int (V_h^*(x) - V_{h+1}^*(\pi_h^*(x))) d((\bar{\pi}_{h-1})_{\#} \nu_{\text{src}})(x) \\ &\leq \frac{H+1}{2} \sum_{h=0}^H \int \|\pi_h^*(x) - x\|^2 d(\bar{\pi}_{h-1})_{\#} \nu_{\text{src}}(x) \end{aligned}$$

where the inequality uses feasibility of V^* . We must thus for each h have equality almost everywhere:

$$V_h^*(x) - V_{h+1}^*(\pi_h^*(x)) = \frac{H+1}{2} \|\pi_h^*(x) - x\|^2.$$

Hence, by feasibility $V_h^*(x) \leq \min_{y \in \Omega} \left(\frac{H+1}{2} \|x - y\|^2 + V_{h+1}^*(y) \right) \leq \frac{H+1}{2} \|\pi_h^*(x) - x\|^2 + V_{h+1}^*(\pi_h^*(x)) = V_h^*(x)$ so we must have equality, which shows both $V_h^*(x) = \min_{y \in \Omega} \left(\frac{H+1}{2} \|x - y\|^2 + V_{h+1}^*(y) \right)$ and that $\pi_h^*(x)$ is a minimizer. \square

B.4 Time scaling

We have seen in the previous sections that the discrete-time dynamic OT problem is equivalent to both the static OT problems (11,10) and the dynamic OT problem (3). The former problem formulation is recovered in our setting by choosing $H = 0$. On the other hand, our formulation can be intuitively viewed as a time-discretization at scale $1/(H + 1)$ of the continuous-time Benamou–Brenier formulation (3). As we argue below, these connections can be extended to accommodate discrete-time formulations at various time scales as well.

The following result shows that further discretizing the time horizon recovers the same optimal transport map but at a finer discretization level (which one may also see by combining Theorem 3.2 and Theorem B.2). The result is a strict generalization of Theorem B.3 (by setting $H' = 0$), but we state and prove it separately for clarity and to highlight the connection to the Benamou–Brenier formulation.

Lemma B.4. *Let $H \in \mathbb{Z}_{>0}$ and $H_k \in \mathbb{Z}_{\geq 0}$ be such that $H_k + 1 = k(H + 1)$, and let us define $h_k = kh$ for all $h \in \{0, 1, \dots, H\}$. Let V^{*,H_k} be optimal for the dynamic dual (Dual LP) with horizon H_k . Then, there is an optimal solution $V^{*,H}$ for the dynamic dual (Dual LP) with horizon H such that*

$$V_h^{*,H} = V_{h_k}^{*,H_k} \quad (h = 0, \dots, H + 1).$$

Proof. For the proof, let us suppose that V^{*,H_k} is an optimal solution to (Dual LP) with horizon H_k , and let $\tilde{V}^{*,H}$ be defined for all $h = 0, \dots, H + 1$ as

$$\tilde{V}_h^{*,H} = V_{h_k}^{*,H_k}.$$

Below, we will show that $\tilde{V}^{*,H}$ is both feasible and optimal for (Dual LP) with horizon H , which will imply the statement of the lemma.

Feasibility: For any $x, y \in \mathbb{R}^d$ set $x_\ell = (1 - \frac{\ell}{k})x + \frac{\ell}{k}y$ (for $\ell = 0, \dots, k$) and notice that by feasibility of V^{*,H_k} , we have

$$\begin{aligned} \tilde{V}_h^{*,H}(x) &= V_{h_k}^{*,H_k}(x_0) \\ &\leq \frac{H_k + 1}{2} \|x_0 - x_1\|^2 + V_{h_{k+1}}^{*,H_k}(x_1) \\ &\leq \dots \\ &\leq \frac{H_k + 1}{2} \sum_{\ell=0}^{k-1} \|x_\ell - x_{\ell+1}\|^2 + V_{k(h+1)}^{*,H_k}(x_k) \\ &= \frac{H_k + 1}{2} \sum_{\ell=0}^{k-1} \left\| \frac{1}{k}(x - y) \right\|^2 + \tilde{V}_{h+1}^{*,H}(y) \\ &= \frac{H_k + 1}{2k} \|x - y\|^2 + \tilde{V}_{h+1}^{*,H}(y) \\ &= \frac{H + 1}{2} \|x - y\|^2 + \tilde{V}_{h+1}^{*,H}(y), \end{aligned}$$

thus implying that $\tilde{V}^{*,H}$ is feasible for (Dual LP) with horizon H .

Optimality: Let $\text{OPT}_{D,H'}^{\text{dyn}}$ denote the optimal value of (D) for horizon H' . We already know from Theorem B.3 that

$$\text{OPT}_{D,H}^{\text{dyn}} = \text{OPT}_D = \text{OPT}_{D,H_k}^{\text{dyn}}. \quad (15)$$

Moreover, by construction $\tilde{V}_0^{*,H} = V_0^{*,H_k}$ and $\tilde{V}_{H+1}^{*,H} = V_{H_k+1}^{*,H_k}$, so by optimality of V^{*,H_k} , we have

$$\begin{aligned} \text{OPT}_{D,H_k}^{\text{dyn}} &= \int V_0^{*,H_k}(x) d\nu_{\text{src}}(x) - \int V_{H_k+1}^{*,H_k}(x) d\nu_{\text{tgt}}(x) \\ &= \int \tilde{V}_0^{*,H}(x) d\nu_{\text{src}}(x) - \int \tilde{V}_{H+1}^{*,H}(x) d\nu_{\text{tgt}}(x). \end{aligned}$$

Plugging this into Eq. (15) concludes the proof. \square

Equivalence between discrete-time and continuous-time dynamic OT. The above theorem suggests that refining the discretization of the time horizon does not change the structure of the optimal value functions and that in the limit, we should recover a potential that corresponds to a straight continuous-time transportation path between ν_{src} and ν_{tgt} , as is known to be the case for the Benamou–Brenier formulation. We make this precise in the following (Corollary B.2), first introducing several simple auxiliary definitions and results (Lemmas B.5 to B.7).

As before, assume that $\text{supp}(\nu_{\text{src}}), \text{supp}(\nu_{\text{tgt}}) \subset \Omega$ for some compact convex $\Omega \subset \mathbb{R}^d$. For $f \in \mathcal{C}(\Omega)$, we define the s -scaled Bellman operator \mathcal{T}_s acting on f via

$$[\mathcal{T}_s f](x) = \min_{y \in \Omega} \left(\frac{\|x - y\|^2}{2s} + f(y) \right)$$

for $s > 0$ and $\mathcal{T}_0 f = f$. We first give an alternative characterization of the optimal value functions which will be useful to establish convergence in the continuous-time limit.

Lemma B.5. *Let (W_0^*, W_1^*) an optimal solution for the static dual problem (13), chosen such that $W_0^* = \mathcal{T}_1 W_1^*$ on all of Ω . Further, set $t(h, H) = h/(H+1)$ for $h = 0, \dots, H+1$ and set $V_h^{*,H} = \mathcal{T}_{1-t(h,H)} W_1^*$. Then, $V^{*,H}$ is optimal for (Dual LP) with horizon H .*

Proof. First, note that we can indeed choose W^* such that $W_0^* = \mathcal{T}_1 W_1^*$ on all of Ω : By optimality, we have $W_0^* = \mathcal{T}_1 W_1^*$ on $\text{supp}(\nu_{\text{src}})$, and by continuity of W_0^* and $\mathcal{T}_1 W_1^*$, we can choose a continuous extension to all of Ω preserving this equality.

Next, it is straightforward to verify that for $s, s' \geq 0$, we have $\mathcal{T}_{s'} \circ \mathcal{T}_s = \mathcal{T}_{s+s'}$ (by convexity of Ω). Using this, we see that for any $h = 0, \dots, H$ and $x \in \Omega$, we have

$$V_h^{*,H}(x) = \mathcal{T}_{1-h/(H+1)} W_1^*(x) = \mathcal{T}_{1/(H+1)} \mathcal{T}_{1-(h+1)/(H+1)} W_1^*(x) = \mathcal{T}_{1/(H+1)} V_{h+1}^{*,H}(x),$$

that is, $V^{*,H}(x) = \min_{y \in \Omega} \left(\frac{H+1}{2} \|x - y\|^2 + V_{h+1}^{*,H}(y) \right)$. In addition, by compactness of Ω and continuity of W_1^* , the value functions $V_h^{*,H}$ are continuous and thus feasible. Finally, $V_0^{*,H} = \mathcal{T}_1 W_1^* = W_0^*$ and $V_{H+1}^{*,H} = W_1^*$, so the objective value of $V^{*,H}$ in the dynamic dual is the same as that of W^* in the static dual, which is optimal by Theorem B.3. \square

We next show that the optimal value functions converge to their continuous-time counterparts as we refine the discretization appropriately.

Lemma B.6. *Let $t \in [0, 1]$ and consider $(h_k, H_k)_{k \geq 1}$ such that for all k , we have $h_k \in \{0, \dots, H_k\}$ and $\frac{h_k}{H_k+1} \rightarrow t$ as $k \rightarrow \infty$. Then for all $x \in \Omega$, $V_{h_k}^{*,H_k}(x)$ from Lemma B.5 converges to $\mathcal{T}_{1-t} W_1^*(x)$ as $k \rightarrow \infty$.*

Proof. We first claim that for any $x \in \Omega$, the map $s \mapsto \mathcal{T}_s W_1^*(x)$ is continuous on $[0, 1]$. For $s, s' > 0$, we have $|\mathcal{T}_s W_1^*(x) - \mathcal{T}_{s'} W_1^*(x)| \leq \frac{\text{diam}(\Omega)^2}{2 \min\{s, s'\}^2} |s - s'|$, showing continuity at every $s > 0$. For $s = 0$, consider a sequence $s_n \rightarrow 0$ ($n \rightarrow \infty$) and notice that by boundedness of $W_1^*(x)$, any minimizer y_{s_n} in the definition of $\mathcal{T}_{s_n} W_1^*(x)$ must satisfy $\|x - y_{s_n}\| \rightarrow 0$. Hence by continuity of W_1^* , we have $\mathcal{T}_{s_n} W_1^*(x) = \frac{\|x - y_{s_n}\|^2}{2s_n} + W_1^*(y_{s_n}) \geq W_1^*(y_{s_n}) \rightarrow W_1^*(x)$ as $n \rightarrow \infty$. On the other hand, we have $W_1^*(y_{s_n}) + \frac{\|x - y_{s_n}\|^2}{2s_n} = \min_{y \in \Omega} \left(\frac{\|x - y\|^2}{2s_n} + W_1^*(y) \right) \leq W_1^*(x)$. Hence $\limsup_{n \rightarrow \infty} \mathcal{T}_{s_n} W_1^*(x) \leq W_1^*(x) \leq \liminf_{n \rightarrow \infty} \mathcal{T}_{s_n} W_1^*(x)$ and thus $\mathcal{T}_{s_n} W_1^*(x) \rightarrow W_1^*(x) = \mathcal{T}_0 W_1^*(x)$ as $n \rightarrow \infty$, showing continuity at $s = 0$.

Hence, we find that for any $x \in \Omega$,

$$V_{h_k}^{*,H_k}(x) = \mathcal{T}_{1-h_k/(H_k+1)} W_1^*(x) \rightarrow \mathcal{T}_{1-t} W_1^*(x) \quad (k \rightarrow \infty)$$

as claimed. \square

Lemma B.7. *Let M^* be a solution to the static OT problem (11). Let $x \in \text{supp}(\nu_{\text{src}})$ and $t \in [0, 1]$ and suppose that $x_t = (1-t)x + tM^*(x) \in \text{int}(\Omega)$. Then $\mathcal{T}_{1-t} W_1^*$ is differentiable at x_t with gradient $\nabla_x \mathcal{T}_{1-t} W_1^*(x_t) = x - M^*(x)$.*

Proof. Let $x \in \text{supp}(\nu_{\text{src}})$ and set $x_t = (1-t)x + tM^*(x)$. Recall that $\mathcal{T}_{1-t} W_1^*(x_t) = \min_{y \in \Omega} \left(\frac{1}{2(1-t)} \|x_t - y\|^2 + W_1^*(y) \right)$. Now for all $y \in \Omega$, we have $W_1^*(y) \geq W_0^*(x) - \frac{1}{2} \|x - y\|^2$ by feasibility of W^* . Hence

$$\begin{aligned} \frac{1}{2(1-t)} \|x_t - y\|^2 + W_1^*(y) &\geq W_0^*(x) + \frac{1}{2(1-t)} \|x_t - y\|^2 - \frac{1}{2} \|x - y\|^2 \\ &= W_0^*(x) - \frac{t}{2} \|M^*(x) - x\|^2 + \frac{t}{2(1-t)} \|y - M^*(x)\|^2, \end{aligned}$$

where the last equality simply follows from noticing $x_t - y = -((y - M^*(x)) + (1-t)(M^*(x) - x))$ and $x - y = -((M^*(x) - x) + (y - M^*(x)))$ and expanding the squares. The final term is non-negative and zero if and only if $y = M^*(x)$. Furthermore, the above inequality is an equality in this case by optimality of W^* (c.f. Theorem B.2). Hence $M^*(x)$ is the unique minimizer in the definition of $\mathcal{T}_{1-t} W_1^*(x_t)$. Hence, by Danskin's theorem, $\mathcal{T}_{1-t} W_1^*$ is differentiable at x_t if $x_t \in \text{int}(\Omega)$, with

$$\nabla_x \mathcal{T}_{1-t} W_1^*(x_t) = \frac{1}{1-t} (x_t - M^*(x)) = x - M^*(x).$$

This concludes the proof. \square

From Lemmas B.6 and B.7 we can immediately deduce the following.

Corollary B.2. *Let $(V_{h_k}^{*,H_k})_{k \geq 1}$ be the optimal value functions for (Dual LP) from Lemma B.6 such that $h_k/(H_k + 1) \rightarrow t \in [0, 1]$ as $k \rightarrow \infty$. Let M^* be an optimal solution for the static OT problem (11). Then, for any $x \in \text{supp}(\nu_{\text{src}})$ such that $x_t = (1-t)x + tM^*(x) \in \text{int}(\Omega)$, we have $V_{h_k}^{*,H_k}(x_t) \rightarrow V_t^\infty(x_t)$ ($k \rightarrow \infty$) for a differentiable function V_t^∞ with*

$$\nabla V_t^\infty(x_t) = x - M^*(x).$$

As shown by Benamou and Brenier [6], the optimal solution to the dynamic OT problem (3) is exactly given by the vector field u_t mapping x_t to $M^*(x) - x$ in the notation of Corollary B.2. Thus, the corollary above implies that the optimal value functions of the dynamic dual problem (D) converge (pointwise) to a well-defined limit that is differentiable, and whose gradient corresponds to the (negative of the) optimal vector field in the Benamou–Brenier formulation—thus connecting the solutions of the discrete-time and continuous-time dynamic OT problems.

C Further implementation details

We now discuss the handful of additional details about the practical implementation of our training and generation methods that did not fit into Sections 3.2 and 3.3.

C.1 Details of VDT training

The two main components of our VDT training algorithm are the primal and dual updates. These are performed in our practical implementation as follows.

Primal updates. The updates are performed according to Equation (7) for a total of K steps with a constant stepsize. In addition to the gradient updates, we have found it useful to add a small amount of Gaussian noise to each update, partly to fight the non-convexity of the primal objective. Indeed, note that the particles move along gradients of a function that is inherently non-convex with respect to the state. Additionally, due to the well-known connection between such noisy Wasserstein gradient descent steps and entropy-regularized sampling [23, 61], this step can be seen as implicitly adding a small amount of entropy regularization to the primal objective in terms of μ . We note though that the type of entropy regularization that this step adds to our OT problem is distinct from the regularization appearing in the famous Schrödinger bridge problem [48] that serves as the basis of many modern generative models. Instead, our regularization acts on the marginal distributions μ_h as opposed to the joint distributions of trajectories, which is known to achieve distinct regularization effects in Markov decision processes—see Neu et al. [38] for more details.

For initializing the particles, our preferred choice is to compute an optimal-transport coupling of the sample $(X_{\text{src}}(i), X_{\text{tgt}}(i))_{i=1}^b$ in the minibatch. For this purpose, since the two particle clouds are of identical size, we can simply employ a standard solver for deterministically matching the two sets. In our implementation, we use the classic Hungarian algorithm for solving this problem (as implemented in the `linear_sum_assignment` function of SciPy [60]).

Dual updates. In all our experiments, we use the stochastic gradients computed in Equation (8) to update parameters using the Adam optimization algorithm [25].

C.2 Details of VDT prediction

Generating samples using VDT policies is straightforward via Algorithm 2. We provide a few additional details about the enhancements of this subroutine below.

Few-step generation. For the purpose of few-step generation, we parametrize our value functions to take inputs in the unit interval, by normalizing the value of h as $t_h = \frac{h}{H+1}$. This is straightforward to incorporate in both the training and generation subroutines (and in fact, Algorithm 2 already adopts this notational convention). Choosing the prediction horizon H_{test} can be seen to be analogous to choosing the hyperparameters of the numerical integration subroutine required by all continuous time models (such as diffusion and flow-based models). In light of our results in Section B.4, our choice can be seen as a simple forward Euler discretization of the continuous-time dynamic OT solution path, which suggests that one can possibly incorporate other advanced ideas from numerical integration into our generation subroutine. We did not pursue this direction in the present paper.

Classifier-free guidance. Classifier-free guidance (CFG,[20]) is a popular technique for improving the sample quality of conditional generative models. At a high level, a small fraction of samples is used for unconditional training, and at inference time the sampling direction of the unconditional model is corrected by a scaled version of the difference between proposed directions of the conditional and unconditional model. This idea can be easily incorporated into our setup by adding the same correction term to the VDT generation process, in particular by changing the generation steps for a *guidance scale* $\alpha > 0$ as

$$X_{h+1} = X_h - \frac{1}{H+1} (\alpha \nabla_x V_h^{\text{conditional}}(X_h) + (1 - \alpha) \nabla_x V_h^{\text{unconditional}}(X_h)).$$

In particular, no changes to conditional training are needed except for not labeling a small fraction ($p_{\text{uncond}} = 0.2$ in our experiments) of training samples.

D Experiments

This section provides further details on our experiments, as well as some additional results that were omitted from the main text. For each setting, we will describe all the hyperparameters (neural network architecture for the value functions and optimizer settings), the data sets and the evaluation procedures.

All experiments were executed on two academic-size clusters with GPU nodes. In particular, 2 NVIDIA H100 GPUs ($\sim 96\text{GB}$ of available GPU memory) from one HPC cluster and 2 NVIDIA L40s from another one ($\sim 45\text{GB}$ of available GPU memory). Each experiment was run on a single GPU, and the more compute-intensive experiments were performed on a single NVIDIA H100 (whose memory was never used to completion by our experiments).

D.1 2D experiments

We implement our method using a three-layer neural network with 64 units per layer to represent a value function, and add a 32-dimensional time embedding layer to encode the time input h . We tune the remaining hyperparameters as follows. For training, we set the batch size as $B = 100$ and perform $T = 20,000$ dual updates using Adam with hyperparameters $\eta_0 = 10^{-4}$, $\beta_1 = 0.9$, $\beta_2 = 0.999$ and $\epsilon = 10^{-8}$. Within the inner loop, we perform $K = 5$ updates with constant stepsize $\gamma = 0.5$ and a noise scale of $\alpha = 10^{-3}$.

We use the following data sets, all taken from Tong et al. [58] (with some additional details extracted from Shi et al. [51] and the associated code repositories):

- “moons”: We use the standard “two moons” data set as implemented in scikit-learn [40], with noise parameter set to 0.05 and each datapoint x transformed as $3x - 1$ for scaling purposes.
- “scurve”: We use the standard “scurve” data set as implemented in scikit-learn [40], with noise parameter set to 0.05 and each datapoint x transformed as $1.5x$ for scaling purposes.
- “8gauss”: We set up eight Gaussian distributions with means evenly spaced on a circle of radius 5 centered at the origin. The standard deviation of each Gaussian is set to 0.1.
- “moons-8gauss”: We use the “moons” and “8gauss” datasets described above, scaled up with a factor 2.

For evaluation, we closely follow the setup of Shi et al. [51]. We set the sample size as $n = 10,000$ and repeat each experiment 5 times and report the means along with the standard deviations in Table 2. For computing the Wasserstein distances (necessary both for evaluating generation quality and computing the oracle solution for the path energies), we use the Hungarian algorithm over a fresh sample batch of 10,000 samples.

All competing methods are based on integrating continuous-time ODEs or SDEs, and thus require a numerical method for approximating the learned transport maps. The numbers we report are based on a forward Euler discretization for 20 steps. Our method does not explicitly require tuning such a hyperparameter, although the role of H_{test} for few-step generation is similar. For a well-trained model, setting $H_{\text{test}} = 10$ worked nearly as well in our experiments as using the default choice $H_{\text{test}} = H = 100$.

Dataset	Wasserstein-2 distance from target				Path energy			
	moons	scurve	8gaussians	moons-8gaussians	moons	scurve	8gaussians	moons-8gaussians
100 step VDT+	0.131±0.034	0.120±0.013	0.435±0.123	0.652 ±0.151	1.238 ±0.059	1.629±0.027	14.386±0.135	30.444 ±0.311
50 step VDT+	0.131±0.034	0.120±0.012	0.434 ±0.123	0.646 ±0.148	1.238 ±0.059	1.629 ±0.027	14.380 ±0.136	30.400 ±0.310+
20 step VDT+	0.131±0.032	0.122±0.013	0.430±0.115	0.634 ±0.131	1.237 ±0.059	1.627±0.026	14.354 ±0.138	30.258 ±0.301
10 step VDT+	0.132 ±0.029	0.125±0.013	0.424±0.111	0.626 ±0.097	1.236 ±0.058	1.623±0.026	14.290±0.148	29.989±0.278
5 step VDT+	0.135 ±0.022	0.136±0.013	0.430 ±0.089	0.623±0.065	1.228±0.057	1.606±0.026	14.067±0.152	29.376 ±0.231
2 step VDT+	0.160 ±0.008	0.178 ±0.012	0.530±0.050	0.783±0.046	1.184 ±0.062	1.531±0.028	13.025±0.145	27.194±0.177
1 step VDT+	0.229 ±0.008	0.262±0.004	0.809±0.025	1.365±0.039	1.066 ±0.073	1.358 ±0.026	10.817 ±0.254	22.679 ±0.333
100 step VDT	0.219±0.086	0.208±0.016	0.547±0.120	1.205 ±0.125	2.416 ±0.096	3.051±0.084	17.799±0.328	73.001 ±2.228
50 step VDT	0.221 ±0.085	0.205±0.015	0.546±0.110	1.229 ±0.1	2.403 ±0.096	3.043±0.082	17.822 ±0.324	73.487 ±2.249
20 step VDT	0.242 ±0.072	0.213±0.030	0.545 ±0.102	1.283±0.062	2.366 ±0.092	3.016 ±0.072	17.886 ±0.326	74.677 ±2.099
10 step VDT	0.307±0.035	0.273±0.058	0.565±0.073	1.360 ±0.077	2.272 ±0.073	2.955 ±0.07	18.046±0.332	76.488 ±2.682
5 step VDT	0.45 ±0.046	0.457±0.052	0.724 ±0.098	1.553±0.099	2.07±0.098	2.761 ±0.062	18.282±0.361	78.488 ±3.955
2 step VDT	0.8 ±0.024	0.958 ±0.084	1.504±0.209	2.757 ±0.043	1.324 ±0.056	1.432 ±0.094	18.115±2.170	66.712 ±3.355
1 step VDT	1.497 ±0.046	1.803±0.048	4.152 ±0.099	6.498 ±0.058	1.154 ±0.061	0.82 ±0.036	0.419 ±0.072	43.230 ±4.396
SF ² M+	0.124±0.023	0.128±0.005	0.275±0.058	0.726±0.137	1.183±0.043	1.686±0.039	14.66±0.173	31.36±0.930
SF ² M	0.185±0.028	0.201±0.062	0.393±0.054	1.482±0.151	2.08 ±0.146	3.01±0.173	16.74±0.274	107.3±9.695
DSBM-IPF	0.140±0.006	0.140±0.024	0.315±0.079	0.812±0.092	1.598±0.034	2.110±0.059	14.91±0.310	42.16±1.026
DSBM-IMF++	0.123±0.014	0.130±0.025	0.276±0.030	0.802±0.172	1.594±0.043	2.116±0.018	14.88±0.252	41.09±1.206
DSBM-IMF	0.144±0.024	0.145±0.037	0.338±0.091	0.838±0.098	1.580±0.036	2.092±0.053	14.81±0.255	41.00±1.495
DSB	0.190±0.049	0.272±0.065	0.411±0.084	0.987±0.324	-	-	-	-
SB-CFM	0.129±0.024	0.136±0.030	0.238±0.044	0.843±0.079	1.649±0.035	2.144±0.044	15.08±0.209	45.69±0.661
FM	0.212±0.025	0.161±0.033	0.351±0.066	-	2.227±0.056	2.950±0.074	18.12±0.416	-
CFM	0.215±0.028	0.171±0.023	0.370±0.049	1.285±0.314	2.391±0.043	3.071±0.026	18.00±0.090	116.5±2.633
OT-CFM+	0.130±0.016	0.144±0.028	0.303±0.043	0.601±0.027	1.216±0.01	1.675±0.019	14.88±0.389	30.47±0.300
RF	0.283±0.045	0.345±0.079	0.421±0.071	1.525±0.330	1.269±0.088	1.793±0.107	15.06±0.447	36.11±2.701
oracle	-	-	-	-	1.123±0.01	1.631±0.03	14.43±0.045	30.02±0.076

Table 2: Sampling quality as measured by Wasserstein-2 distance to target and path energy for the 2D experiments. We report the mean and standard deviation of 5 independent runs, with best results highlighted in bold (somewhat generously, to help guide the attention of the reader). Results for all competing methods taken from Tong et al. [58]. Methods marked with “+” use an OT coupling for forming minibatches, and methods using a full OT plan over the entire data set for initialization are marked with “++”.

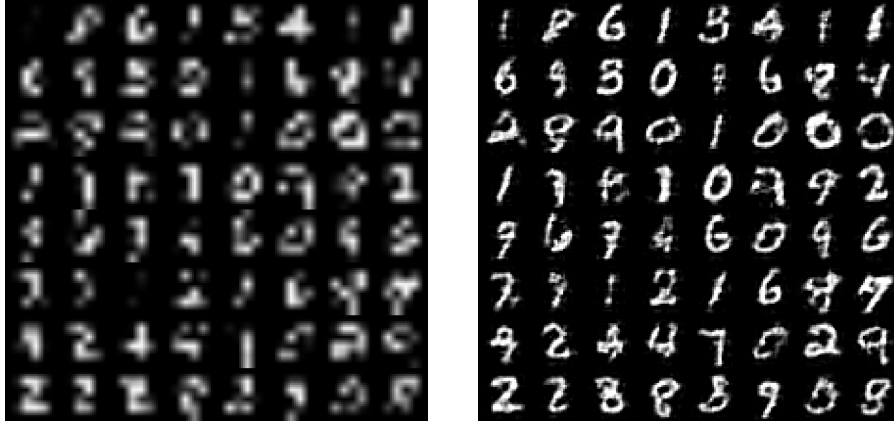


Figure 5: Downscaled images and their deblurred counterparts produced by VDT, $m = 6$.



Figure 6: Downscaled images and their deblurred counterparts produced by VDT, $m = 10$.

D.2 MNIST experiments

In this set of experiments, we work with the classic MNIST data set [27], comprised of 28×28 greyscale images of handwritten digits, represented as vectors with dimension $d = 784$. For all experiments, we use a convolutional neural network with 832, 289 trainable parameters. For VDT training, we set the batch size as $B = 128$ and perform $T = 20,000$ dual updates using AdamW with hyperparameters $\eta_0 = 10^{-3}$, $\beta_1 = 0.0$, $\beta_2 = 0.999$ and $\epsilon = 10^{-8}$, and a weight decay parameter of 10^{-2} . Within the inner loop, we perform $K = 5$ updates with constant stepsize $\gamma = 0.25$ and a noise scale of $\alpha = 10^{-3}$.

Paired deblurring. For the deblurring experiments, we downsample the original 28×28 MNIST images to dimension $m \times m$ and linearly upsample them back to the original full dimension. The resulting blurred image $X_{\text{src}}(i)$ is paired with its original counterpart $X_{\text{tgt}}(i)$ during VDT training. We train a model for $m = 6, 10, 14$ each and evaluate the result on a holdout set of unseen blurred MNIST images. In addition to the results shown in the main paper, further results are presented on Figures 5–7.

Unpaired letter to digit translation. We next consider a task without naturally available pairings, namely the one of translating handwritten letters (‘a’-‘e’ and ‘A’-‘E’ from EMNIST [10]) to handwritten digits (0-9 from MNIST). We train a VDT model on unpaired minibatches of letters and digits, and evaluate the result on a holdout set of unseen letters in Section 4.2. While the sharpness of the generated digits could likely be improved through heavier training, they clearly exhibit the desired resemblance of the source letters. In short, VDT is able to learn a nontrivial relation between the domains without explicit supervision. Notably, this relation naturally allows for generation along the reverse path (i.e. from digits to letters) without any additional training, as we remarked



Figure 7: Downsampled images and their deburred counterparts produced by VDT, $m = 14$.

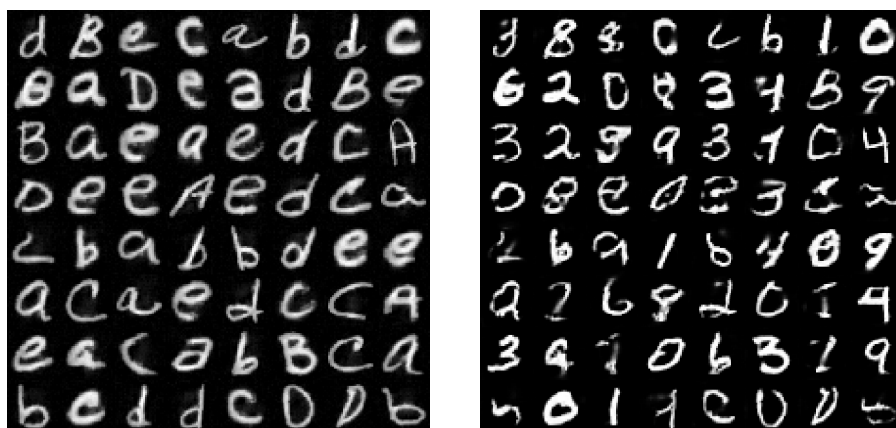


Figure 8: Forward sampling from a VDT policy from EMNIST to MNIST.

previously. Additionally, the straightness of the VDT paths allow for few-step translation between the two distribution, with some example outputs shown in the main text. We show some additional examples in Figures 8 and 9.

Conditional generation of MNIST digits We apply the CFG procedure explained in Appendix C to our setting for generating MNIST images augmented with their class labels. Results for various



Figure 9: Reverse sampling from a VDT policy from MNIST to EMNIST.

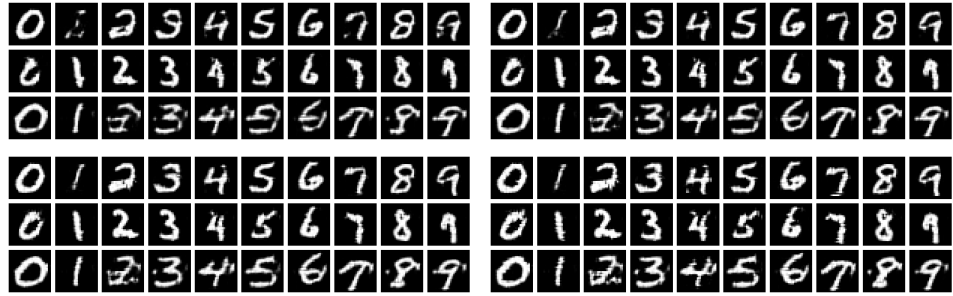


Figure 10: MNIST digits generated by CFG with various guidance scales: $\alpha \in \{1.0, 1.5, 2.0, 3.0\}$.

scale parameters are shown on Figure 10. The results indicate that CFG affects the generation quality in the same way as it does for diffusion models: we obtain enhanced image quality at the expense of smaller sample diversity.